MASTERARBEIT | MASTER'S THESIS

Titel | Title

Molecular Dynamics Simulation of the Gβ1γ2 Complex Carrying the L30F Mutation Associated with GNB1 Encephalopathy

verfasst von | submitted by

Gabriele Habison BSc

angestrebter akademischer Grad | in partial fulfilment of the requirements for the degree of

Magistra pharmaciae (Mag. pharm.)

Wien | Vienna, 2025

Studienkennzahl lt. Studienblatt | Degree programme code as it appears on the student record sheet:	UA 066 605
Studienrichtung lt. Studienblatt | Degree programme as it appears on the student record sheet:	Masterstudium Pharmazie
Betreut von | Supervisor:	Assoz. Prof. Mag. Dr. Anna Weinzinger Privatdoz.

Acknowledgements

I would like to express my sincere gratitude to Assoc. Prof. Mag. Dr. Anna Weinzinger, Privatdoz., for her excellent supervision and for welcoming me into her research group. I am truly grateful for the opportunity to complete my Master's thesis under her guidance and for all the valuable experiences I gained during this exciting time.

My deepest thanks go to Ilia Steshin, who supervised me throughout my thesis, he always took the time to answer my questions and helped me with every concern.

I would also like to thank the entire Division of Pharmacology and Toxicology.

An exceptional thank you goes to my family, my parents and siblings, for their continuous support and motivation throughout my studies. I deeply appreciate that you have always been there for me. None of this would have been possible without you.

I am also immensely grateful to my friends and fellow students. Thanks to you, even the most stressful times were much more bearable.

I am truly thankful to all of you!

Abstract

GNB1 encephalopathy is a rare neurodevelopmental disorder caused by mutations in the GNB1 gene, which encodes the Gβ1 subunit of heterotrimeric G proteins. Among these mutations, the L30F mutation has shown divergent clinical characteristics compared to other pathogenic variants. This study investigates the structural and dynamic consequences of the L30F mutation on the Gβ1γ2 complex using molecular dynamics (MD) simulations.

Simulations of both the wildtype and mutant forms were performed to assess differences in free energy, structural stability and flexibility. Analyses included calculations of ΔΔG, root mean square deviation (RMSD), root mean square fluctuation (RMSF) and residue-residue interactions based on non-equilibrium MD approaches.

The results suggest that the L30F mutation does not significantly destabilize the Gβ1γ2 complex, with only minor structural deviations and local fluctuations observed. A calculated ΔΔG value of –2.74 kJ/mol indicates only a slight stabilizing effect. These findings align with previous functional assays, which showed no significant impairment of G protein interactions.

Residue-residue interaction analysis identified four Gγ2-residues, Val30, Ala34, Leu37, and Met38, that interact with L30F and are important for local stabilization.

This study offers structural information regarding the potential molecular impact of the L30F mutation and points out the value of further investigations focusing on downstream signaling pathways, which may explain the observed pathogenic effects.

Zusammenfassung

Die GNB1-Enzephalopathie ist eine seltene neurologische Entwicklungsstörung, die durch Mutationen im GNB1-Gen verursacht wird, welches für die Gβ1-Untereinheit von heterotrimeren G-Proteinen codiert. Unter diesen Mutationen zeigt die Variante L30F ein abweichendes klinisches Erscheinungsbild im Vergleich zu anderen pathogenen Varianten. Diese Arbeit untersucht mithilfe molekulardynamischer (MD) Simulationen die strukturellen und dynamischen Auswirkungen der L30F-Mutation auf den Gβ1γ2-Komplex. Sowohl Wildtyp als auch Mutante wurden simuliert, um Unterschiede in freier Energie, Protein-Stabilität und Flexibilität zu analysieren. Die Auswertung umfasste die Berechnung von ΔΔG, Root Mean Square Deviation (RMSD), Root Mean Square Fluctuation (RMSF) sowie der Aminosäuren-Interaktionen auf Basis nicht-gleichgewichts MD-Simulationen.

Die Ergebnisse deuten darauf hin, dass die L30F-Mutation den Gβ1γ2-Komplex nicht signifikant destabilisiert. Es wurden lediglich geringfügige strukturelle Abweichungen und lokale Fluktuationen beobachtet. Der berechnete ΔΔG-Wert von –2,74 kJ/mol weist auf eine nur leicht stabilisierende Wirkung hin. Diese Befunde stimmen mit früheren funktionellen Studien überein, die keine signifikante Beeinträchtigung der G-Protein-Interaktionen ergaben.

Die Analyse der Aminosäuren-Interaktionen identifizierte vier Gγ2-Aminosäuren, Val30, Ala34, Leu37 und Met38, die mit L30F interagieren und zur lokalen Stabilisierung beitragen könnten.

Diese Arbeit liefert strukturelle Einblicke in die potenziellen molekularen Auswirkungen der L30F-Mutation und unterstreicht die Notwendigkeit weiterführender Untersuchungen zu nachgeschalteten Signalwegen, die möglicherweise die beobachteten pathogenen Effekte erklären.

Table of Contents

Acknowledgements……I
Abstract……..II
Zusammenfassung……III
List of abbreviations……VI
List of figures……..VII
List of tables……...VIII
1 Literature Overview 1
1.1 GNB1-Encephalopathy 1
1.1.1 Clinical Manifestations 1
1.1.2 Genetic Inheritance 1
1.1.3 Therapeutic Approaches 1
1.2 G protein-coupled receptors and G-proteins 2
1.2.1 Gβγ Subunit Diversity and Expression 3
1.2.2 Structure of the Gβγ subunits 5
1.2.3 Gβγ influence on GIRK channels 6
1.3 Functional and Structural Characterization of the GNB1 L30F Mutation 7
1.4 Molecular Dynamics Simulations 12
1.4.1 The basics of MD 13
1.4.2 Advantages of MD Simulations 15
1.4.3 Limitations and Challenges 15
1.5 Calculation of Free Energy Changes upon Amino Acid Mutation 17
2 Objective 22
3 Materials and Methods 24
3.1 Simulation programs 24
3.1.1 pmx 24
3.2 MD Simulation Process 25

3.3 Analysis of Residues in Contact with Gβ L30 27
3.4 Sequence Alignment of Human Gγ Subunits 28
4 Results 32
4.1 Free Energy Calculation for the Tripeptide with the L30F Mutation 33
4.2 Free Energy Calculation for the Gβ1γ2 Subunit with the L30F Mutation 35
4.3 ΔΔG Calculation Results 37
4.4 Root Mean Square Deviation (RMSD) 38
4.5 Root Mean Square Fluctuation (RMSF) 38
4.6 Residue Energy Analysis 39
5 Discussion 43
6 Conclusion 45
7 References 46
8 Internet References 50
9 Supplementary Material 51

List of abbreviations

BAR	Bennet Acceptance Ratio
BiFC	Bimolecular Fluorescence Complementation
BRET	Bioluminescence Resonance Energy Transfer
CADD	Combined annotation dependent depletion
CFT	Crooks Fluctuation Theorem
Cryo-EM	Cryo-electron microscopy
D1R	Dopamine 1 receptor
F	Phenylalanin
GDD	Global devvelopmental delay
GDP	Guanosine diphosphate
GIRK	G protein gated inwardly rectifiering potassium (channel)
GNB1	Guanine nuclotide binding protein beta 1
GNB1-E	GNB1 Encephalopathy
GPCR	G protein coupled receptor
GPUs	Graphics processing units
GTP	Guanosine triphosphate
Gβ1	G protein subunit beta 1
ID	intellectual disability
L	Leucin
LJ	Lennard-Jones
MD	Molecular dynamics
MUT	Mutation
NEW	Non-equilibrium work
PDB	Protein data bank
RGS	Regulators of G protein signaling
RMSD	Root mean square deviation
RMSF	Root mean square fluctuation
VMD	Visual Molecular Dynamics
WT	Wildtype
ΔΔG	Change in Gibbs Free Energy

List of Figures

Figure 1: G protein-coupled receptors send signals by using soluble G proteins 3
Figure 2: Crystal structure of the Gβγ dimer and G protein heterotrimer 5
Figure 3: A diagram showing how GPCR activates GIRK channels 6
Figure 4: Schematic representation of the amino acid Leucin and Phenylalanin..... 7
Figure 5: Mutant residues in Gβ1γ2 dimer found in dystonia patients 8
Figure 6: Clinical, genetic and functional data of 16 individuals carrying the mutation. 9
Figure 7: Effect of missense mutations on Gβ1γ7 dimer formation..... 9
Figure 8: Bioluminescence Resonance Energy Transfer (BRET) assay..... 10
Figure 9: Extended cell-based BRET assay to monitor D1R-stimulated G protein activation. 11
Figure 10: Schematic representation of a thermodynamic cycle used to calculate changes in protein folding free energy upon mutation 21
Figure 11: Gβ1γ2 complex extracted from PDB 4KFM 25
Figure 12: WT-structure – L30 in Gβ1 interacts within a 10 Å radius with residues in Gγ2 27
Figure 13: Residue comparison of all human Gγ subunits..... 28
Figure 14: Free energy calculation for the tripeptide model with the L30F mutation 35
Figure 15: Free energy calculation for the Gβ1γ2 subunit with the L30F mutation 37
Figure 16: RMSD of the Gβ1 subunit for 250 ns MD simulation..... 38
Figure 17: RMSF of the Gβ1 subunit for 250 ns MD simulation 39
Figure 18: L30F-Residue interactions of the last 50 ns of the simulation process..... 40
Figure 19: L30F-Residue interactions of the 250 ns simulation process. 40
Figure 20: Coulomb energy for 250 ns simulation time for L30F-residues interactions. ... 41
Figure 21: Lennard-Jones Energy for 250 ns simulation time for L30F-residues interactions. 41
Figure 23: Comparison of residue 30, 34, 37 and 38 in Gγ subunits. 42

List of Tables

Table 1: Gγ subunits tissue-specific expression 4
Table 2: Gγ-residues (10 Å radius of L30 in Gβ) 27
Table 3: Gγ subunits structures created with VMD and AlphaFold server 29
Table 4: MD Simulation Results for the Tripeptide 32
Table 5: MD Simulation Results for the Gβγ subunit 33
Table 6: Calculated ΔΔG Values 37

1 Literature Overview

1.1 GNB1-Encephalopathy

GNB1 encephalopathy (GNB1-E) is a very rare genetic disorder caused by pathogenic variants in the guanine nucleotide-binding protein beta 1 (GNB1) gene, which encodes the G protein subunit beta 1 (Gβ1) (Lohmann et al., 2017; Revah-Politi et al., 2021). Fewer than 100 cases have been reported globally to date (www1). The GNB1 gene is recognized as one of the genes associated with neurodevelopmental disorders (Petrovski et al., 2016).

1.1.1 Clinical Manifestations

The clinical phenotype of GNB1-E is typically marked by moderate to severe developmental delay and intellectual disability. A broad range of neurological symptoms has been observed, including abnormalities in muscle tone, movement or eye movement disorders, epilepsy, and sensory impairments (Nasvytis et al., 2024; Revah-Politi et al., 2021). To date, only one mutation has been found that does not have developmental delay, which is the L30F mutation (Lohmann et al., 2017).

1.1.2 Genetic Inheritance

Most individuals diagnosed with GNB1-E carry a de novo mutation in the GNB1 gene, meaning the variant arose spontaneously rather than being inherited. The condition follows an autosomal dominant inheritance pattern. In nearly all cases where parental genetic testing was conducted, the mutation was absent in both parents. However, the recurrence risk in siblings is higher compared to the general population, primarily due to the possibility of parental germline mosaicism (Revah-Politi et al., 2021).

1.1.3 Therapeutic Approaches

Currently, no curative treatment exists for GNB1-E. Therefore, symptom management remains the primary approach. Due to the wide range of developmental and intellectual impairments, early multidisciplinary intervention is essential. Infants may benefit from feeding support, physiotherapy, occupational therapy, and specialized sensory input. For older children, individualized education plans, psychological therapy, ongoing physical therapy, and assistive mobility devices are often necessary (Nasvytis et al., 2024; Revah-Politi et al., 2021).

Epileptic seizures in individuals with GNB1-E are generally treated with standard antiepileptic drugs. But the type of epilepsy can vary greatly among these patients and not all of them are adequately managed with the therapy they receive (Hemati et al., 2018). While no specific agent has been identified as most effective, ethosuximide showed efficacy in reducing epileptiform activity in a mouse model (Colombo et al., 2023).

Movement disorders and dystonia are typically managed using established protocols involving anticholinergic drugs, dopamine-modulating agents, benzodiazepines, or baclofen (Bledsoe et al., 2020). Since the disease is very rare, treatment plans are highly individualized, and clinical outcomes can vary significantly (Revah-Politi et al., 2021).

1.2 G protein-coupled receptors and G-proteins

G protein-coupled receptors (GPCRs) represent the largest family of membrane-bound receptor proteins found in eukaryotic organisms. The human genome contains over 800 different genes that encode GPCRs, reflecting their extensive functional diversity. These receptors are distributed widely across different tissues and are essential for regulating a wide range of physiological processes (Wootten et al., 2018).

G proteins (guanine nucleotide-binding proteins) are intracellular signal transducers that play a central role in relaying messages from activated GPCRs at the cell surface to downstream intracellular targets. Structurally, G proteins exist as heterotrimers, comprising three distinct subunits: alpha (α), beta (β), and gamma (γ). The α-subunit possesses GTPase activity and is responsible for binding and hydrolyzing guanine nucleotides (GTP = guanosine triphosphate and GDP = guanosine diphosphate). The β and γ subunits remain tightly associated as a functional βγ complex, which is also crucial for intracellular signaling (Hamm, 1998).

Upon binding an extracellular ligand, the GPCR undergoes a conformational shift, which activates the associated G protein. This activation enables the α-subunit to exchange GDP for GTP. Once bound to GTP, the G protein dissociates into two parts: the GTP-bound α-subunit and the βγ dimer. Both components can independently interact with and regulate various effector proteins, such as enzymes or ion channels, triggering diverse cellular responses. The signal is eventually terminated when the Gα subunit hydrolyzes GTP to GDP.

This reaction restores the inactive state, allowing the α-subunit to recombine with the βγ complex and reassemble the heterotrimeric G protein (Smrcka, 2008). The activation cycle is illustrated in Figure 1.

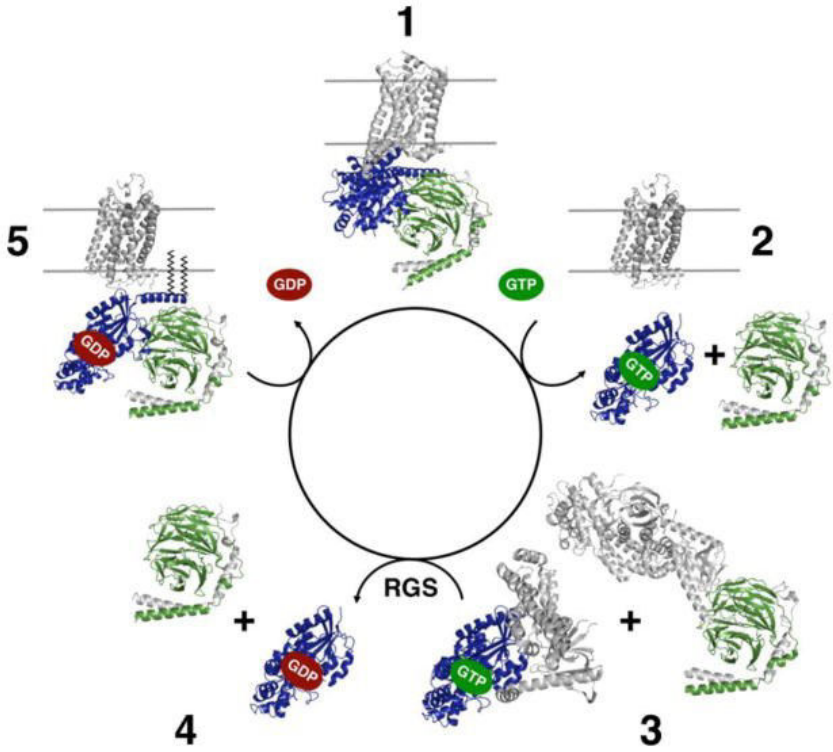

Figure 1: G protein-coupled receptors (GPCRs) send signals by using soluble G proteins. In the resting state, the heterotrimeric G protein is composed of α, β, and γ subunits, with GDP bound to the α subunit (State 1). Upon ligand binding to a GPCR, the receptor undergoes a conformational change into GTP-bound Gα, and Gβγ (State 2). Both are able to bind to downstream effectors to propagate the signal (State 3). Regulators of G protein Signaling (RGS) proteins enhance the intrinsic GTPase activity of the Gα subunit. Following GTP hydrolysis, the GDP-bound form of Gα re-associates with the Gβγ dimer (State 4). The resulting complex then returns to the plasma membrane, where it interacts with receptors and participates in a new signaling cycle (State 5). (Thaker et al., 2012).

1.2.1 Gβγ Subunit Diversity and Expression

The human genome encodes five distinct genes for Gβ subunits (Gβ1–Gβ5) and twelve for Gγ subunits (Gγ1–Gγ13, excluding Gγ6). While Gβ1 to Gβ4 exhibit a high degree of sequence similarity (greater than 80%), Gβ5 is structurally distinct, sharing only about 50% sequence identity with the other isoforms. In contrast, Gγ subunits are even more diverse, with sequence similarities ranging from 20% to 80%. This high degree of variability is believed to be a major factor contributing to the functional specificity of different Gβγ heterodimers (Tennakoon et al., 2021).

A particularly important region within the Gγ subunit, the amino acid residues 36 to 49, has been identified as essential for its interaction with Gβ subunits (Spring & Neer, 1994). Among the Gβ isoforms, Gβ1 is unique in its capacity to form heterodimers with all known Gγ subtypes. Moreover, Gβ1 is ubiquitously expressed across mammalian tissues and shows the highest expression levels among Gβ subunits in nearly all examined human tissues. Expression is especially pronounced in regions such as the putamen and the small intestine (Betke et al., 2014; Tennakoon et al., 2021).

The cell- and tissue-specific expression patterns of Gγ subunits further underscore their role in driving the functional diversity of Gβγ signaling. Each Gγ isoform is expressed in a distinct set of tissues, suggesting specialized roles in different physiological contexts. Table 1 summarizes the tissue-specific expression patterns of the individual Gγ subunits, as reported by Kankanamge et al. (2022).

In rod and cone photoreceptor cells of the retina, the heterotrimeric G-protein transducin is essential for signal transmission. The γ-subunit of transducin exists in cell-type-specific forms: Gγ1 (also GγT1; encoded by GNGT1) is found in rods, and Gγ9 (also Gγc or GγT2; encoded by GNGT2) is restricted to cones (Ong et al., 1997; Kolesnikov et al., 2022).

Table 1: Gγ subunits tissue-specific expression

Gγ subunits	**Tissue-specific expression**
Gγ1	Retina
Gγ2	Brain, smooth muscles
Gγ3	Brain
Gγ4	Brain, endocrine tissue
Gγ5	Ubiquitous
Gγ7	Brain
Gγ8	Brain
Gγ9	Retina
Gγ10	Ubiquitous
Gγ11	Endocrine, liver, muscle tissue
Gγ12	Placenta, fat tissue, bronchus
Gγ13	Brain, retina

1.2.2 Structure of the Gβγ subunits

The Gβ1 subunit assemble into a characteristic β-propeller structure, with four-stranded β sheets forming each of the seven blades of the propeller (Figure 2A). At the N-terminus the first 57–70 amino acids form the α-helical domain of the β-propeller. This helix participates in a tightly packed coiled-coil interaction with the Gγ2 subunit. The β sheets of the propeller and the variable loops connecting the β strands, the most conserved regions within Gβ. The Gα subunit contains two structurally independent elements that interact with different sites on the Gβγ complex. One interaction site involves the N-terminal α-helix of Gα, which contacts the lateral surface of blade 1 on the β-propeller. A second point of contact is formed by the switch II region of Gα, which undergoes conformational changes upon GTP binding and interacts with the upper side of the β-propeller (Figure 2B) (Sondek et al., 1996; Smrcka, 2008).

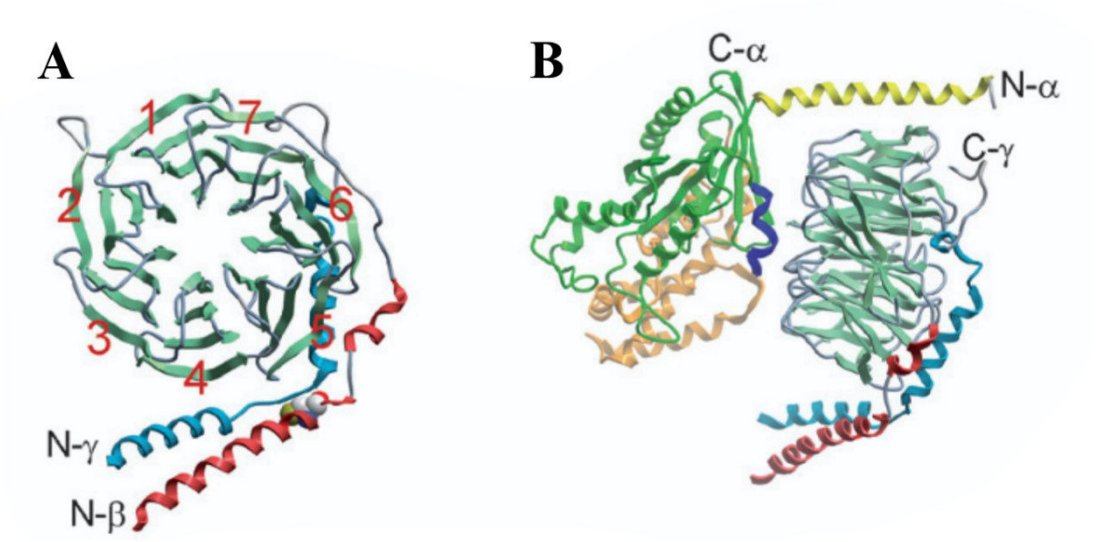

Figure 2: (A) Crystal structure of the Gβγ dimer. The blades of the propeller are numbered from 1 to 7. The Gβ N-terminal helix, depicted in red, interacts with the Gγ subunit (shown in blue) through a coiled-coil formation. (B) G protein heterotrimer. The Gα N-terminus is depicted as a yellow helix, while the Gα Switch II region is shown in dark blue (Smrcka, 2008).

Several specific residues within Gβ have been identified as key contact points for Gα binding, including positions 57, 78, 80, 89, and 110. These same residues, along with others, are also implicated in interactions with downstream signaling proteins. For instance, lysine 78 (K78) and arginine 96 (R96) have been shown to play important roles in the association between the Gβ1γ2 complex and G protein-gated inwardly rectifying potassium (GIRK) channels (Reddy et al., 2021).

Structural data in the Protein Data Bank (www5) are currently limited to complexes containing the Gβ1 subunit with Gγ2 or GγT1. Consequently, there is no information about the structures of Gβ1 in combination with other Gγ subunits. GγT1 is the γ-subunit of the heterotrimeric G-protein transducin, located in the rod photoreceptors of the retina and is also described as Gγ1 (Odds et al., 1997).

1.2.3 Gβγ influence on GIRK channels

Among the numerous downstream targets regulated by GPCR activation, the Gβγ dimer directly modulates several key effector proteins. These include G protein-gated inwardly rectifying potassium (GIRK) channels (GIRK1–4; also known as Kir3.1-Kir3.4), voltage-gated calcium channels (Ca_V), presynaptic SNARE proteins, specific isoforms of adenylyl cyclase, phospholipase Cβ, phosphoinositide 3-kinase γ (PI3Kγ), and G protein-coupled receptor kinases (GRKs) (Guo et al., 2002; Reddy et al., 2021).

Figure 3 illustrates the mechanism by which Gβγ activates GIRK channels. Following ligand binding, the GPCR undergoes a conformational change that facilitates the exchange of GDP for GTP on the Gα subunit of the heterotrimeric G protein. This nucleotide exchange leads to the dissociation of the G protein from the receptor, followed by the separation of the Gα subunit from the Gβγ dimer. The free Gβγ complex then interacts with cytoplasmic domains of the GIRK channel. This interaction is strongly dependent on the presence of phosphatidylinositol 4,5-bisphosphate (PIP_2), a membrane phospholipid that is essential for stabilizing the open state of the channel. In addition to Gβγ-mediated activation, GIRK channels can also be activated by increased intracellular concentrations of sodium ions (Na^+), which act as an additional modulator of channel gating (Whorton & MacKinnon, 2013).

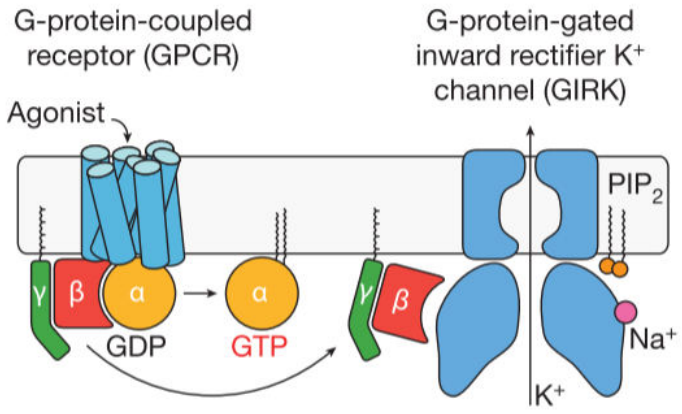

Figure 3: A diagram showing how GPCR activates GIRK channels (Whorton & MacKinnon, 2013).

Reddy et al. (2021) investigated three Gβ1 mutations (K78R, I80N, and I80T) using both computational and experimental methods. In heterologous expression systems, these mutations did not disrupt the coupling of GPCRs to $G_{i/o}$ proteins or the regulation of the neuronal voltage-gated calcium channel $Ca_V2.2$ by Gβγ. However, they significantly altered the Gβγ-mediated regulation of GIRK channels. These effects involved changes in Gβ1 expression levels, Gβγ binding to the cytoplasmic regions of GIRK subunits, and Gβγ function. The K78R mutation led to a gain-of-function, while I80T and I80N resulted in loss-of-function, with effects varying depending on the specific GIRK subunit involved.

1.3 Functional and Structural Characterization of the GNB1 L30F Mutation

The L30F mutation results in the substitution of leucine with phenylalanine at position 30 (Figure 4). Although both amino acids are hydrophobic, leucine contains a nonpolar aliphatic side chain, whereas phenylalanine has a bulkier aromatic side chain (Müller-Esterl, 2018).

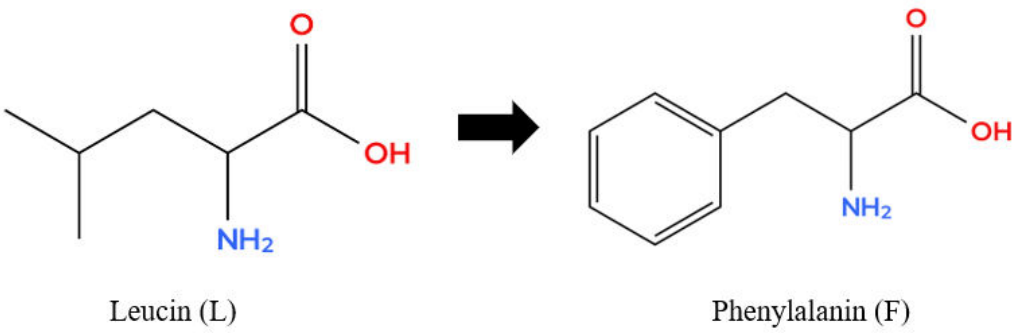

Figure 4: Schematic representation of the amino acid Leucin (left) and Phenylalanin (right). Molview (www2) was used to create the figure.

The missense mutation L30F (leucine to phenylalanine at position 30) stands out among the GNB1 variants identified in the study by Lohmann et al. (2017) because it differs from other Gβ1 mutations in structural positions, genetics, and clinical picture.

The positions of ten Gβ1 mutations in the Gβγ complex are shown in Figure 5. The amino acid residues R52, A92, P94, R96, and D118 are positioned near the interaction sites with Gα or effector molecules. On the other hand, the likely benign variants L30F, H91R, and K337Q are situated further away from these interaction surfaces. This structural placement indicates minimal impact on protein function for the L30F mutation.

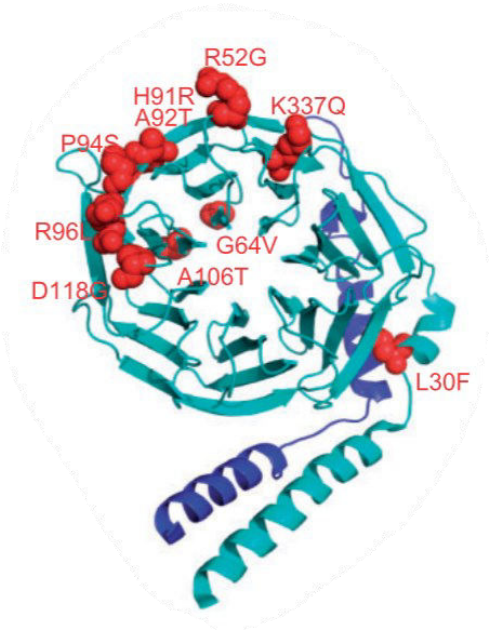

Figure 5: Mutant residues in Gβ1γ2 dimer found in dystonia patients are highlighted in red (Lohmann et al., 2017).

In Figure 6, there is a summarized presentation of all patients analyzed in this study, along with clinical, genetic, and functional information. L30F is the only mutation that is located in exon 4. The patient carrying L30F did not show signs of global developmental delay (GDD), which was otherwise observed in all other patients with functionally confirmed pathogenic GNB1 mutations. Furthermore, the patient shows growth delay, muscular hypotonia, intellectual disability, seizures, nystagmus and ataxia (Lohmann et al., 2017).

Case	1	2	3	4	5	6	7	8	9	10	11	12	13	14	15	16
Sex	M	F	F	M	M	M	F	M	F	F	M	M	F	M	F	M
Age at diagnosis	4	2.5	4	2.4	5	8	2.9	4	6	1	Unk	8	12	8	6	8
Ethnicity	Saudi Arabian	Qatar	Egypt	Saudi Arabian	Israeli	Mexican	Saudi Arabian	Kuwaiti	Israeli	Indian	Mexican	Algerian	German	Saudi Arabian	Indian	Saudi Arabian
Var Build 19	1:1749284	1:1747244	1:1747207	1:1736021	1:1736013	1:1736016	1:1736014	1:1736008	1:1736001	1:1736001	1:1736001	1:1735972	1:1735935	1:1720492	1:1718877	1:1718784
NM_002074	c.88C>T	c.154C>G	c.191G>T	c.268-1G>T	c.272_275del	c.272A>G	c.274G>A	c.280C>T	c.287G>T	c.287G>T	c.287G>T	c.316G>A	c.353A>G	c.915_916del	c.917-1G>T	c.1009A>C
NP_002065	p.L30F	p.R52G	p.G64V	p.?	p.?	p.H91R	p.A92T	p.P94S	p.R96L	p.R96L	p.R96L	p.A106T	p.D118G	p.?	p.?	p.K337Q
Location of mut.	Exon 4	Exon 5	Exon 5	Intron 6	Exon 7	Exon 7	Exon 7	Exon 7	Exon 7	Exon 7	Exon 7	Exon 7	Exon 7	Exon 10	Intron 10	Exon 11
Type of mut.	ms	ms	ms	ss	fs	ms	ms	ms	ms	ms	ms	ms	ms	fs	ss	ms
Change in function	No	Yes	Yes	Not tested	Not tested	No	Yes	Yes	Yes	Yes	Yes	Yes	Yes	Not tested	Not tested	No
CADD score (v1.3)	22	21	33	27	35	18	25	23	26	26	26	24	29	35	26	24
Inheritance	*De novo*	*De novo*	*De novo*	*De novo*	*De novo*	Unk	*De novo*	Unk	Dominant	Dominant	Dominant	*De novo*	*De novo*	*De novo*	Unk	*De novo*
GDD	No	Yes	Yes	Yes	Yes	Yes	Yes	Yes	Yes	Yes	Yes	Yes	Yes	Yes	Yes	Yes
Growth delay	Yes	No	No	No	Yes	Yes	No	No	Yes	No	No	No	No	No	Yes	No
Muscular hypotonia	Yes	No	No	Yes	No	Yes	Yes	No	No	No	No	No	Yes	Yes	Yes	No
ID	Yes	Yes	No	Yes	Yes	Yes	Yes	Yes	No	Yes	Yes	No	Yes	Yes	Yes	Yes
Seizures	Yes	No	No	No	Yes	Yes	Yes	No	Yes	No	Yes	Yes	No	Yes	Yes	Yes
Cranniosynostosis	No	No	No	Yes	Yes	No	No	No	No	No	No	Yes	No	No	No	No
Cerebellar hypoplasia	No	Yes	No	No	No	Yes	Yes	No	No	No	No	No	No	No	No	No
Abnormal myelination	No	No	No	Yes	Yes	No	No	No	Yes	No	Yes	No	No	Yes	No	Yes
Ophthalmoplegia	No	Yes	No	Yes	No	No	No	Yes	Yes	No	No	No	No	No	No	No
Nystagmus	Yes	Yes	No	No	Yes	Yes	No	No	Yes	No	Yes	No	No	Yes	Yes	Yes
Ataxia	Yes	Yes	No	No	Yes	No	Yes	No	No	No	No	No	No	No	Yes	No
Chorea	No	No	No	No	No	No	No	Yes	No	No	No	No	No	No	No	No
Dystonia	No	No	No	No	No	No	No	No	No	No	No	No	Yes	No	No	No

Figure 6: Clinical, genetic and functional data of 16 individuals carrying the mutation. The L30F mutation is framed in red. Unk = unknown, ss = splice site, fs = frameshift, ms = misssense, GDD = global developmental delay, ID = intellectual disability, CADD = combined annotation dependent depletion (Lohmann et al., 2017).

To assess the impact of ten GNB1 missense variants on D1R signaling via the $G\alpha_{olf}\beta_1\gamma_7$ complex, their effect on the assembly of Gβ1–Gγ7 dimers was analyzed using a bimolecular fluorescence complementation (BiFC) assay. Gγ7 was selected due to its prominent role in $G\alpha_{olf}$-mediated signaling within the striatum, a brain region critically involved in various neurological conditions, including movement disorders (Schwindinger, 2010). In this approach, the successful interaction between Gβ1 and Gγ7 leads to the reconstitution of the Venus fluorescent protein, allowing detection through fluorescence intensity measurements (Figure 7) (Lohmann et al., 2017).

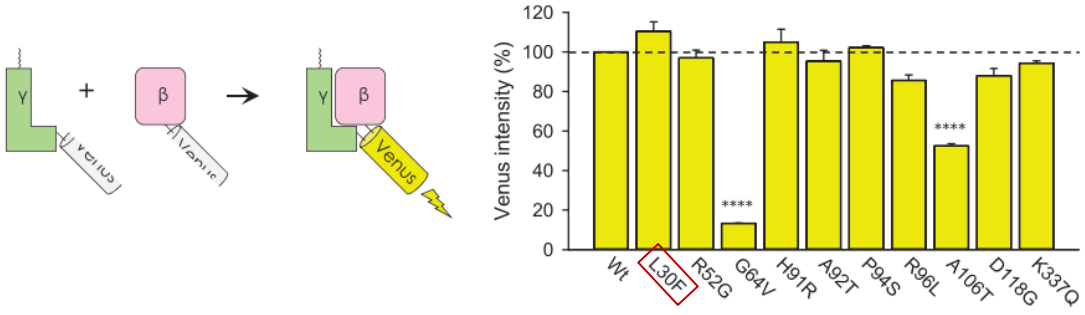

Figure 7: Effect of missense mutations on Gβ1γ7 dimer formation.
Left: Schematic presentation of the BiFC assay for testing Gβγ dimer formation. Two non-fluorescent fragments of Venus are attached to Gβ and Gγ. When Gβ and Gγ interact, the fragments come together and form a yellow fluorescent protein called Venus. Right: Quantitative evaluation of Gβ1γ7 dimer formation in Gβ1 mutants, Venus intensity was measured (Lohmann et al., 2017).

Subsequently, the influence of the missense variants on the interaction between Gβ1γ7 and $G\alpha_{olf}$ was investigated using a cell-based bioluminescence resonance energy transfer (BRET) assay. In this setup, the Venus-tagged Gβ1γ7 dimer associates with a luciferase-linked GRK reporter, generating a measurable BRET signal. The addition of $G\alpha_{olf}$ competes with the GRK reporter for binding to the Venus-Gβ1γ7 complex, resulting in a decrease in BRET signal, this is a sign that the $G\alpha_{olf}$–Gβ1γ7 heterotrimer is successfully forming (Figure 8).

Variants G64V and A106T, previously identified as impairing Gβ1γ7 dimerization, showed significantly lower basal BRET signals. Additionally, the P94S and R96L mutations led to a moderate reduction in BRET intensity, indicating a partial disruption of trimer formation. In contrast, the A92T variant produced a higher basal BRET signal, which also points to impaired heterotrimer assembly. However, the L30F variant showed BRET levels comparable to the wildtype, suggesting that trimer formation was unaffected.

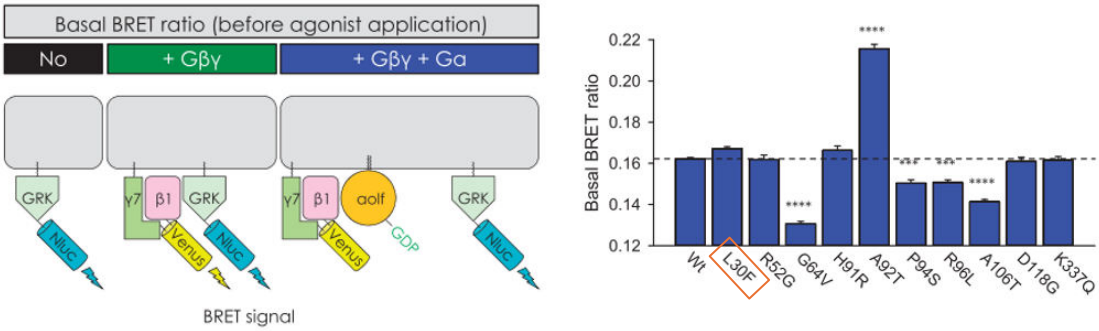

Figure 8: Bioluminescence Resonance Energy Transfer (BRET) assay.
Left: Schematic representation of the assay used to measure basal BRET levels, prior to agonist stimulation, to assess Gαβγ trimer formation. Expression of Gα subunit reduces the BRET signal by displacing the GRK reporter, whereas disruption of trimer formation increases the BRET signal. Right: Basal BRET ratios for the ten tested GNB1 missense variants (Lohmann et al., 2017).

To evaluate the functional responsiveness of the GNB1 variants upon receptor activation, an advanced cell-based BRET assay was utilized (Figure 9). In this model, stimulation of the dopamine 1 receptor (D1R) triggers dissociation of the $G\alpha_{olf}$-Gβ1γ7 heterotrimer, leading to a rapid rise in the BRET signal. This increase reflects the capacity of the Gβ1γ7 complex to engage in downstream signaling upon receptor activation.
Deficient mutants, such as A92T, R52G and G64V, exhibited significant alterations in BRET signals relative to the wild type, indicating deficits in receptor-driven G protein activation. In contrast, the L30F and H91R variants displayed normal signaling behavior, showing no functional deviations from the wildtype Gβ1 (Lohmann et al., 2017).

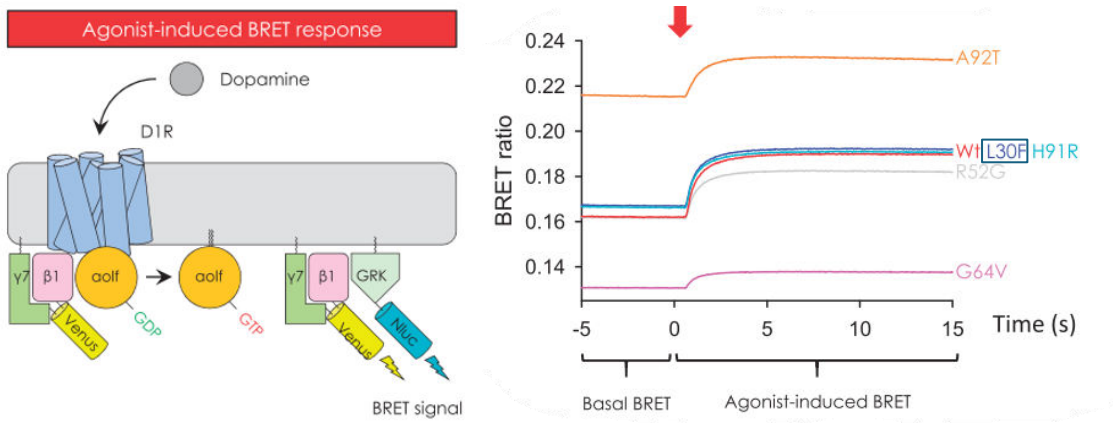

Figure 9: Extended cell-based BRET assay to monitor D1R-stimulated G protein activation.
Left: Schematic overview of the assay. Dopamine stimulation triggers dissociation of the Gαolf–Gβγ heterotrimer. The released Venus-tagged Gβγ subunits bind to the GRK-Nluc reporter, resulting in an increased BRET signal. Right: A red arrow marks the point of dopamine application (Lohmann et al., 2017).

Although the L30F variant did not exhibit any detectable functional impairments in the assays employed in this study, it cannot be ruled out that this mutation may influence Gβ1 function under physiological conditions or in molecular contexts not assessed here. Such effects could involve altered interactions with alternative effector proteins or with different Gα and Gγ subunits, potentially contributing to pathogenic processes in individuals carrying this variant. Nonetheless, structural modeling indicates that the amino acid substitution lies outside the conserved interaction interface of Gβ1, thereby reducing the likelihood of a direct impact on protein–protein interactions (Lohmann et al., 2017).

1.4 Molecular Dynamics Simulations

Molecular dynamics (MD) simulations have become an essential computational tool used to explore how chemical and biological systems behave over time at the atomic level. The motions of atoms are simulated over time based on laws of physics. MD allows the observation of dynamic processes such as protein folding, conformational transitions, and biomolecular interactions under conditions that are meant to resemble a real biological environment (Bassani & Moro, 2023).

The fundamental principle of MD simulations is simple. Starting from the established three-dimensional coordinates of all atoms in a biomolecular system, for example a protein embedded in water or a membrane environment. It is possible to calculate the net force acting on each atom based on interactions with all other atoms in the system. These forces are then used, according to Newton's laws of motion, to determine how each atom will move over time. By repeating this process in tiny time steps, the simulation continuously recalculates forces and updates atomic velocities and positions. This iterative process generates a time-resolved atomic trajectory that effectively represents a dynamic, three-dimensional visualization of the system's structural evolution (Hollingsworth & Dror, 2018).

The increasing adoption of MD simulations in molecular biology and pharmaceutical research is due to their ability to provide high-resolution, time-dependent insights into the behavior of proteins, nucleic acids, and other biomolecules. Their application has been greatly facilitated by recent advances in hardware performance, improved simulation algorithms, and the expanding availability of experimentally derived molecular structures (Hollingsworth & Dror, 2018). These developments have broadened the use of MD from fundamental structural studies to the rational design and optimization of therapeutic molecules.

In the context of drug discovery, MD serves multiple purposes. It is commonly employed to refine docking results, probe the stability of ligand–target complexes, or elucidate the mechanistic basis of molecular recognition events (Bassani & Moro, 2023). Two major factors have contributed to the widespread use of MD in this field. First, the increasing resolution and availability of structural data, driven by breakthroughs in techniques such as cryo-electron microscopy (cryo-EM) and X-ray crystallography, provide diverse, high-

quality starting structures. Second, MD simulations have become more practical due to improvements in computational power, particularly through the use of graphics processing units (GPUs), which enable complex simulations to be performed on accessible hardware platforms (Hollingsworth & Dror, 2018).

Traditionally, structural input for MD simulations has been obtained from X-ray crystallography, but advances in electron microscopy and NMR spectroscopy have expanded the range of available input data. Cryo-EM, in particular, has emerged as a powerful complement to crystallography, offering detailed structures of complex and flexible systems that were previously difficult to resolve (Bai et al., 2015; Hollingsworth & Dror, 2018).

1.4.1 The basics of MD

Guided by the principles of physics, MD simulations monitor the movement of every single atom in a protein over time by simulating their interactions with each other. A mechanical force field is utilized to calculate the potential energies and forces acting on all atoms in the system, allowing the prediction of its dynamic behavior (Karplus & McCammon, 2002).

Forces can be derived from the potential energy function:

$$\vec{F} = -\nabla U(\vec{r})$$

A force field consists of empirical energy functions and associated parameters that define the potential energy U based on the molecular coordinates. The potential energy function is composed of non-bonded and bonded interactions (www3):

$$U(\vec{r}) = \sum U_{bonded}(\vec{r}) + \sum U_{non-bonded}(\vec{r})$$

Non-bonded interactions include electrostatic and non-electrostatic interactions for each pair of atoms. The Lennard–Jones (LJ) potential models the non-electrostatic energy between non-bonded atoms or molecules:

$$V_{LJ}(r) = \frac{C12}{r^{12}} - \frac{C6}{r^{6}}$$

The r−12 term represent the Pauli repulsion that arises when electron orbitals overlap, while the r−6 term represents the weaker attractive dispersion forces that arises from transient

dipoles in the valence electrons. A common formulation uses the parameters ε (well depth) and σ (van der Waals radius):

$$V_{LJ}(r) = 4\varepsilon\left[\left(\frac{\sigma}{r}\right)^{12} - \left(\frac{\sigma}{r}\right)^{6}\right], \qquad C_{12} = 4\varepsilon\sigma^{12}, \qquad C_6 = 4\varepsilon\sigma^6$$

The Coulomb's law describes the electrostatic potential around a particle:

$$V_{Elec} = \frac{q_i q_j}{4\pi\varepsilon_0\varepsilon_r r_{ij}}$$

The bonded term includes several contributions. The bond potential is expressed as: $V_{Bond} = k_b\left(r_{ij} - r_0\right)^2$, where r_0 is the bond length and k_b the bond constant. The angle potentia: $V_{Angle} = k_\theta\left(\theta_{ijk} - \theta_0\right)^2$, with θ_0 as the bond angle and k_θ the force constant. The torsion (dihedral) angle potential: $V_{Dihed} = k_\emptyset\Big(1 + cos(n_\emptyset - \delta)\Big)$ where *n* is the periodicity and δ the phase shift angle (www3).

By solving Newton's equations of motion over time, the positions and velocities of the atoms are determined, producing a trajectory that captures successive configurations of the system as it evolves (Adcock & McCammon, 2006).
Newton's second law:

$$\mathbf{f}_i(t) = m_i\mathbf{a}_i(t) = -\frac{\partial V(\mathbf{x}(t))}{\partial \mathbf{x}_i(t)}$$

Here, $f_i(t)$ represents the net force acting on atom *i* at time *t*, $a_i(t)$ denotes the corresponding acceleration, and m_i indicates the mass of the atom (De Vivo et al., 2016).

Quantum mechanics describes the motion of atoms, electrons, and molecules, where a wave function obtained by solving the Schrödinger equation represents all system properties (Atkins, 2014):

$$i\hbar\frac{\partial\psi}{\partial t} = \hat{H}\psi$$

In this context, t represents time, ψ denotes the wave function, ħ signifies the reduced Planck constant, and Ĥ refers to the Hamiltonian operator.

The Born–Oppenheimer approximation is needed to separate electronic and nuclear motion by treating the heavier nuclei as stationary during electronic calculations (Adcock & McCammon, 2006). The total wave function is then approximated as

$$\Psi(\mathbf{r}, \mathbf{R}) \approx \psi_{\text{electrons}}(\mathbf{r}; \mathbf{R}) \cdot \chi_{\text{nuclei}}(\mathbf{R})$$

where $\psi_{electrons}$ (r; R) is the electronic wave function calculated for fixed nuclear positions R, and χ_{nuclei}(R) is the nuclear wave function (Atkins, 2014).

1.4.2 Advantages of MD Simulations

One of the real strengths of MD simulations is their ability to offer an atomistic view of biomolecular systems, which enables researchers to investigate molecular mechanisms with exceptional precision. MD allows for the observation of dynamic processes under controlled, replicable conditions, something often difficult to achieve in laboratory experiments. It captures the real-time motion of every atom, which facilitates a more nuanced understanding of events such as allosteric regulation or ligand-induced conformational changes (De Vivo et al., 2016; Hollingsworth & Dror, 2018).

Another major advantage is the increasing accessibility of MD technologies. The proliferation of GPU-accelerated computing and the availability of user-friendly software has made it possible to perform simulations that previously required supercomputers on inexpensive computer chips. This development of computational power has allowed MD simulations to cover longer timescales, extending from nanoseconds to milliseconds, as well as more complex molecular systems (Hollingsworth & Dror, 2018; Lazim et al., 2020).

1.4.3 Limitations and Challenges

Although MD simulations are powerful, they still have some inherent limitations. One significant limitation is due to the approximations used in force fields, which are based on empirical and theoretical models. Inaccurate parameterization can result in incorrect predictions of molecular behavior, particularly when simulating uncommon interactions or unusual chemical environments (Bassani & Moro, 2023; Lazim et al., 2020).

Additionally, standard classical MD cannot directly simulate the formation or breaking of covalent bonds. This limitation becomes relevant in cases involving proton transfer, redox

reactions, or enzyme catalysis, where bond rearrangements are central to the process. In such cases, Quantum Mechanics/Molecular Mechanics (QM/MM) are necessary, but these come with increased computational costs (Bassani & Moro, 2023).

The quality of the starting structure also plays an important role. If the initial protein or ligand conformation is inaccurate, those errors can propagate throughout the simulation and influence the outcome. This makes high-resolution, experimentally validated input data so important when aiming for reliable results (Hollingsworth & Dror, 2018).

Finally, MD simulations are time constrained. Many biologically relevant processes such as protein folding, conformational changes, or ligand binding, take place over microseconds to milliseconds, sometimes even longer. Such timescales are still difficult to reach with routine MD simulations. While improved sampling techniques can partially achieve this, they require careful implementation and can introduce bias. In practice, most MD simulations typically use time steps of only 1–2 femtoseconds with total simulation lengths ranging from nanoseconds to microseconds, depending on the complexity of the system and available computational resources (Lazim et al., 2020).

1.5 Calculation of Free Energy Changes upon Amino Acid Mutation

Free energy plays a central role in thermodynamics and kinetics. Therefore, a key goal of computer-aided molecular design is to accurately predict free energy changes upon amino acid mutations. Various approaches have been developed to estimate the free energy change associated with varying protein stability or binding affinities. These include alchemical free energy methods. These calculations are based on all-atom computer simulations that accurately sample the Boltzmann distribution of microstates while considering entropic and discrete solvent effects (Aldeghi et al., 2019; Serra et al., 2025).

The connection between energies at the molecular level and macroscopic thermodynamic behavior is made by the Boltzmann distribution, which determines the population of molecules across different energy states:

$$N_i \; \alpha \; e^{-\frac{\varepsilon_i}{kT}}$$

where N_i is the population of state i, ε_i is its energy, k is Boltzmann's constant, and T is the absolute temperature (Atkins, 2014).

Two forms of free energy are commonly employed in thermodynamics: the Gibbs free energy and the Helmholtz free energy. The Gibbs free energy, denoted by G, is particularly relevant for systems at constant temperature and pressure, conditions that are typical for most chemical and biological processes. The Gibbs free energy is defined as: $G=H-TS$, where H is the enthalpy, T is the absolute temperature, and S is the entropy of the system. The change in Gibbs free energy, ΔG, provides a direct measure of the spontaneity of a process: $\Delta G=\Delta H-T\Delta S$. A negative value of ΔG indicates a spontaneous process, a positive value implies non-spontaneity, and a zero value corresponds to a system at equilibrium.
The Helmholtz free energy, defined as $A=U-TS$, with U representing the internal energy, applies to systems at constant volume and temperature (Atkins, 2014).

Amino acid transformations can be performed reversibly (in so-called equilibrium free energy calculations) or irreversibly (in non-equilibrium calculations). A particular focus is on the theoretical foundations of non-equilibrium work (NEW) calculations and their application to estimating free energy changes upon amino acid mutation along alchemical (that means non-physical) pathways (Aldeghi et al., 2019).

The free energy surface of a system determines its thermodynamic and kinetic properties, thus enabling the understanding of biophysical processes such as protein folding, ligand binding, and protein-protein association (Xiong et al., 2006).

A protein in solution may adopt a multitude of conformations, ranging from highly disordered to well-structured forms. The ensemble of disordered conformations is typically referred to as the unfolded state (state A), while the ordered conformations constitute the folded state (state B). The difference in free energy ΔG is proportional to the ratio of the probabilities of finding the system in state A or B:

$$\frac{p_A}{p_B} = \frac{e^{-\beta G_A}}{e^{-\beta G_B}} = e^{-\beta(G_A - G_B)}$$

$$\Delta G = G_A - G_B = -k_B T \ln \frac{p_A}{p_B}$$

Here, G represents the free energy of the system, with G_A and G_B corresponding to the free energies of the unfolded (state A) and folded (state B) configurations, respectively. The parameter β is defined as $\beta = \frac{1}{k_B T}$, where k_B is the Boltzmann constant and T the absolute temperature (Serra et al., 2025).

According to the second law of thermodynamics, the average work ⟨W(τ)⟩ performed during a process due to dissipative work is always greater than or equal to the free energy difference ΔG between the initial and final states:

$$\langle W(\tau) \rangle \geq \Delta G$$

Equality holds only in the idealized case of a reversible process, where the system remains in thermodynamic equilibrium throughout the transition.

A non-equilibrium transformation is typically coupled with the parameter λ, which interpolates between the initial and final states of the system. The process is initiated at λ=0

and gradually driven to λ=1, with λ being continuously varied at each simulation timestep (Seeliger & Groot, 2010; Aldeghi et al., 2019). This controlled progression enables the computation of the work performed on the system during the transformation:

$$W(\tau) = \int_{\lambda=0}^{\lambda=1} \frac{\partial \mathcal{H}(\boldsymbol{x}, \boldsymbol{v}, \lambda)}{\partial \lambda} d\lambda$$

Here, H denotes the system's Hamiltonian, which is a function of the phase-space coordinates x, velocities v, and the coupling parameter λ.

In 1997, Jarzynski derived an equation that links the unidirectional nonequilibrium work average and the equilibrium free energy difference:

$$\left\langle e^{-\beta W(\tau)} \right\rangle = e^{-\beta \Delta G}$$

Jarzynski's equality applies to processes carried out in a single direction, typically from λ = 0 to λ = 1 (Jarzynski, 1997).

In contrast, the Crooks Fluctuation Theorem (CFT) extends this framework by incorporating work distributions from both the forward (λ:0→1) and reverse (λ:1→0) processes. This bidirectional approach provides a more statistically robust means of estimating ΔG, especially when there is sufficient overlap between the forward and reverse work distributions (Serra et al., 2025).

According to the CFT, the probability distributions of work values obtained from forward and reverse non-equilibrium processes are related to the equilibrium free energy difference by the following expression:

$$\frac{P_f(W)}{P_r(-W)} = e^{\beta(W - \Delta G)}$$

Here, $P_f(W)$ and $P_r(-W)$ represent the normalized probability distributions of the work performed in the forward and reverse directions, respectively. This relationship allows the

free energy difference to be determined from the point at which the two distributions intersect.

An alternative and widely used estimator is the Bennett Acceptance Ratio (BAR), which does not require an analytical approximation for the work distributions. BAR combines information from both forward and reverse processes to obtain an optimal estimate of the free energy difference (Aldeghi et al., 2019). The following equation is fulfilled:

$$\sum_{i=1}^{N_f} \frac{1}{1 + \frac{N_f}{N_r} e^{\beta(W_i - \widehat{\Delta G})}} = \sum_{j=1}^{N_r} \frac{1}{1 + \frac{N_r}{N_f} e^{-\beta(W_j - \widehat{\Delta G})}}$$

N_f represents the number of forward trajectories, while N_r denotes the number of backward trajectories. This equation must be solved numerically, typically using iterative methods such as the Newton-Raphson or Nelder-Mead algorithms.

To calculate a free energy difference, the system must be defined in terms of two thermodynamic states, an initial state corresponding to the unfolded conformation and a final state representing the folded structure. The free energy difference between these states can be estimated by simulating the transition. If the structure of the folded state is available, a possible strategy involves driving the system from the folded to the unfolded conformation (or vice versa) by, for example, mechanically pulling the N- and C-termini apart and measuring the work performed during this process (Aldeghi et al., 2019).

When the objective is to quantify the change in folding free energy due to a point mutation (denoted as $\Delta\Delta G_{folding}$), a thermodynamic cycle can be employed to facilitate this calculation (Figure 10). This approach utilizes alchemical (non-physical) transformations that involve smaller, localized perturbations instead of simulating the full folding process, which is computationally expensive and slow to converge. These transformations are applied both in the folded and unfolded states of the protein. Because free energy is a state function, the total free energy change is independent of the path taken. This path-independence justifies the use of non-physical, alchemical routes to compute thermodynamic quantities such as folding stability changes (Aldeghi et al., 2019).

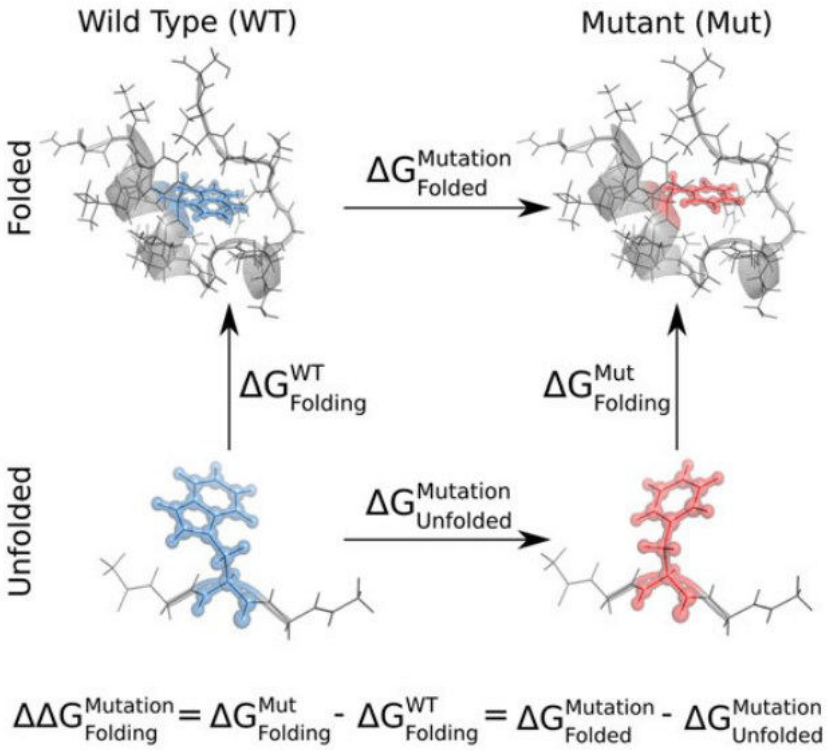

Figure 10: Schematic representation of a thermodynamic cycle used to calculate changes in protein folding free energy upon mutation ($\Delta\Delta G_{Folding}^{Mutation}$) (Aldeghi et al., 2019).

The left column illustrates the folding process of the wildtype protein, associated with a folding free energy $\Delta G_{Folding}^{WT}$. The right column shows the analogous folding process for the mutant, with the folding free energy $\Delta G_{Folding}^{Mut}$. The bottom row represents the alchemical transformation of the wildtype protein in its unfolded state into the mutant with a corresponding free energy change $\Delta G_{Unfolded}^{Mutation}$. The top row depicts the same alchemical transformation but applied to the folded protein, resulting in a free energy difference $\Delta G_{Folded}^{Mutation}$.

While the vertical transitions (physical folding/unfolding) are computationally intensive, the horizontal alchemical transformations are more accessible. Therefore, $\Delta\Delta G_{Folding}^{Mutation}$ can be calculated from the difference between $\Delta G_{Folded}^{Mutation}$ and $\Delta G_{Unfolded}^{Mutation}$ (Aldeghi et al., 2019).

The change in protein folding free energy due to mutation reflects the impact of the mutation on the structural stability of the protein. A positive ΔΔG value ($\Delta\Delta G > 0$) indicates a destabilizing mutation, resulting in a loss of protein stability. Conversely, a negative ΔΔG value ($\Delta\Delta G < 0$) suggests a stabilizing mutation, which leads to an increase in protein stability (Aldeghi et al, 2019).

2 Objective

GNB1-E is a rare and severe neurodevelopmental disorder caused by mutations in the Gβ subunit, which lead to disruptions in G-protein-mediated signaling pathways. To explore the structural implications of the disease-associated L30F mutation, molecular dynamics (MD) simulations were employed. This master's thesis represents an initial step toward understanding how the L30F variant affects the Gβ1γ2 complex.

The simulations were designed to model the Gβ subunit including the L30F mutation, allowing for the identification of structural stability deviations and potential functional consequences. This approach aimed to provide insights into the pathophysiological mechanisms underlying this specific mutation.

To investigate the effects of the L30F mutation on the Gβγ complex and fulfill the research objectives, the following steps were undertaken:

1. The simulation system was prepared using CHARM-GUI, based on the Gβγ complex extracted from the crystal structure with PDB ID 4KFM, and included the L30F mutation.
2. Non-equilibrium MD simulations (ranging from 50 to 200 ps) were conducted using a simplified tripeptide model, followed by simulations of the full Gβ1γ2 complex. Each simulation was performed for both the wildtype and L30F mutant form and repeated five times to ensure reproducibility.
3. Free energy calculations were performed to estimate the thermodynamic impact of the L30F mutation, particularly regarding protein–protein interactions, with the goal of assessing potential changes in complex stability and function.
4. After MD simulation runs were analyzed, we extended the MD simulation run 3 to 250 ns (run 3 was closest to the mean of all 5 runs). It was carefully evaluated using selective parameters such as RMSF (Root Mean Square Fluctuation) and RMSD (Root Mean Square Deviation).
5. Residue-residue interaction energies between L30F and Gγ2 residues were calculated for both the wildtype and the mutant using the extended simulation run. The computed free energy values identify the key residues involved in interactions with L30F.

These efforts mark a foundational step toward understanding the structural and functional consequences of how the L30F mutation influences the behavior of the Gβ1γ2 complex and contributes to the pathophysiology of GNB1 encephalopathy.

3 Materials and Methods

3.1 Simulation programs

Molecular dynamics simulations were performed using GROMACS version 2022.3, which was installed on a system running LINUX Ubuntu version 20.04.6.

3.1.1 pmx

Pmx is a Python library designed to facilitate the generation and manipulation of biomolecular structure and topology files for molecular dynamics simulations (www4). It provides a collection of specialized scripts that automate the setup and analysis of alchemical free energy calculations, particularly in the context of amino acid mutations.

One of the core functionalities of pmx is the generation of hybrid topologies, which are essential for simulating transitions between different molecular states (for example wildtype and mutant proteins). The tool is fully compatible with the GROMACS simulation engine and supports several molecular mechanics force fields. Mutation libraries enable this compatibility by accurately applying residue-specific force field parameters during topology generation.

pmx therefore streamlines complex workflows and is especially useful for high-throughput mutational scanning or the evaluation of mutation-induced free energy differences (Aldeghi et al., 2019; Gapsys et al., 2015).

3.2 MD Simulation Process

The protein structure used in this study was prepared via CHARMM-GUI, based on the Gβ1γ2 complex extracted from the PDB entry 4KFM (www5). PDB 4KFM contains the crystal structure of the G protein-gated inward rectifier K^+ channel GIRK2 (Kir3.2) in complex with the Gβ1γ2 protein subunits, and only the Gβ1γ2 subunits were used in this study (Figure 11).

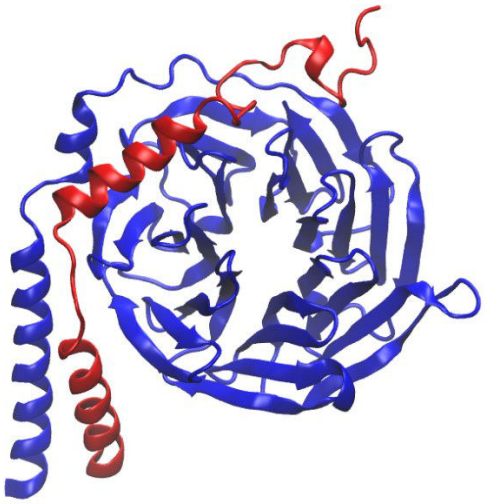

Figure 11: Gβ1γ2 complex extracted from PDB 4KFM (www4). Gβ1 in blue color, Gγ2 in red, shown in VMD.

In MD simulation, atomic interactions are described using a force field to calculate the potential energy of a system at the atomic level. This makes it possible to specify the force acting on each individual atom. The exact positions and velocities of all atoms are updated over a specified period. Thus, the force field contributes to the dynamics of the system. The Amber99SB*ILDN force field was used here. The MD calculation was performed for a protein-in-water system (TIP3P) with an ion concentration of 0.15 mol/L containing Na^+ and Cl^- ions. The TIP3P water model is characterized by its precision when it comes to simulating aqueous environments for their neutralization (Jo et al., 2008). The PMX site (www4) was utilized to create hybrid topologies and tripeptide systems.

The necessary steps for calculating the free energy, including energy minimization, NVT (constant number, volume, temperature), NPT (constant number, pressure, temperature) solvent equilibrium (100 ps), production MD (10 ns), and non-equilibrium MD (50 to 200 ps). Energy minimization is necessary in MD simulations to avoid steric collisions and high-

energy interactions between atoms in the simulation box. This allows the system to start in a stable, low-energy state.

In the next step, called the equilibrium phase, the system must reach equilibrium. At this point, all atoms start in their original positions and configurations. Variables such as pressure and temperature are monitored until a stable state is reached. The first 2 ns of each equilibrium trajectory were excluded as the equilibrium time. In the last 8 ns, 100 evenly spaced frames (1 frame per 80 ps) were extracted, representing an equilibrium set of initial conformations for the non-equilibrium transitions. The required working values for the transitions (WT => L30F and L30F => WT) were documented. The free energy difference between the two states was then determined using the Crooks fluctuation theorem. The free energy was calculated using the BAR (Bennet's Acceptance Ratio) estimator. This method was used for five runs, for the tripeptide and for the protein, starting with the creation of the box.

The Root Mean Square Deviation (RMSD) and Root Mean Square Fluctuation (RMSF) calculations were performed using GROMACS tools for run 3 and extended to 250 ns. The RMSD serves as a tool for analyzing MD simulations. RMSD is used to measure the local distance between two protein structures. The deviation between the protein structure and the original structure is continuously determined. The mean distance between the atoms of the selected molecule at a given time is measured compared to the reference structure. The mean square fluctuation provides an additional tool for investigating MD simulations. The RMSF, which is an indicator of structural flexibility, measures the temporal fluctuation of a specific molecule or atom. It is calculated by determining the spatial variation of the selected residues. It is a crucial factor for identifying residues that remain flexible even after the structure has stabilized.

3.3 Analysis of Residues in Contact with Gβ L30

Residue L30 of the Gβ1 subunit (PDB ID: 4KFM) gets close contacts with residues of the Gγ2 subunit. All Gγ2 residues within a 10 Å distance of L30 were identified using VMD (Figure 12) and are summarized in Table 2. These are the amino acids at positions 29 to 41 in Gγ2.

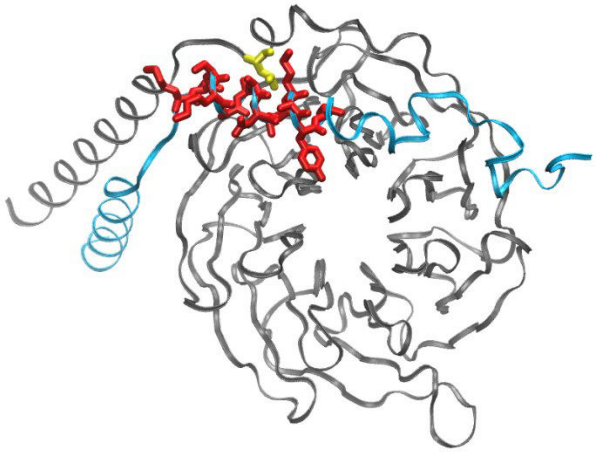

Figure 12: WT-structure – L30 in Gβ1 interacts within a 10 Å radius with residues in Gγ2. Gβ1 in grey, Gγ2 in blue, L30 in yellow, and Gγ2 residues in red, created in VMD with PDB: 4KFM.

Table 2: Gγ-residues (10 Å radius of L30 in Gβ)

Residue number	Aminoacid
29	LYS
30	VAL
31	SER
32	LYS
33	ALA
34	ALA
35	ALA
36	ASP
37	LEU
38	MET
39	ALA
40	TYR
41	CYS

3.4 Sequence Alignment of Human Gγ Subunits

Amino acid sequences of all known human Gγ isoforms (GNG1–GNG13, no GNG6), were retrieved from the UniProt database (www6) in FASTA format and compiled into a single sequence file. This file was then submitted to the MAFFT web server (EMBL-EBI, www7) for multiple sequence alignments. The resulting alignment enabled a direct comparison of variable residues across the Gγ isoform family (Figure 13).

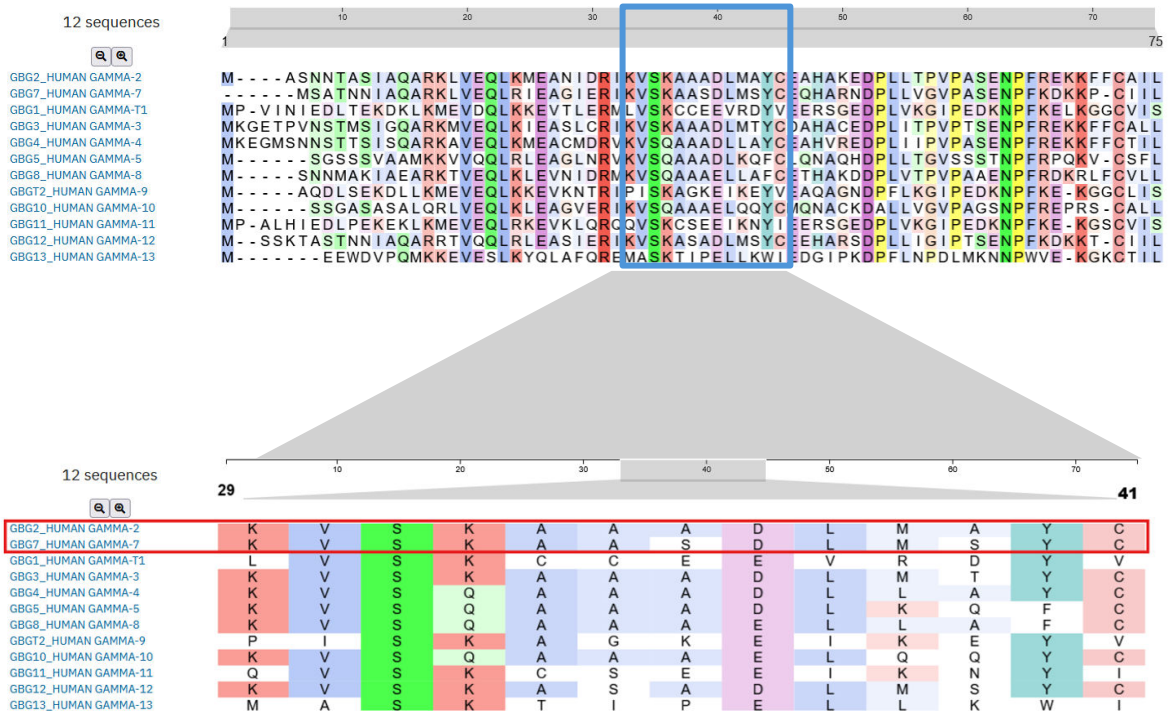

Figure 13: Residue comparison of all human Gγ subunits. Gγ2 and Gγ7 framed in red, sequence alignment with the MAFFT web server (EMBL-EBI, www7).

This analysis is of particular interest because Gβ1 is known to interact with all Gγ isoforms (Tennakoon et al., 2021). The L30F mutation may disrupt specific interactions between Gβ1 and individual Gγ subunits. We used Gβ1γ2 in our calculations, while Lohmann et al. (2017) used Gβ1γ7. A comparison of these two variants reveals that two amino acids differ within a 10 Å radius of the mutation site: residue 35 and 39 are an Alanine (A) in Gγ2 and a Serine (S) in Gγ7. In comparison to all other variants, this critical region shows no identical amino acid composition, there is always at least one different residue, often several.

It should be noted that L30 or F30 of Gβ does not necessarily interact with every amino acid within a 10 Å radius. To investigate this relationship in more detail, additional calculations were performed. Specifically, the energy interactions between L30F and the Gγ2 residues

were calculated for both the wildtype and the mutant. For this residue-residue energy analysis, the extended simulation run was used. Python scripts and GROMACS software were used to estimate residue-residue $U_{non\text{-}bonded}$. The results are presented in the Results part.

An evaluation of potential Gγ subunit structures was performed using AlphaFold (www8). The different Gγ subunits generally show a similar structure (Table 3). The binding site between L30 and Gγ (residue 29 to 41) seems to be structurally conserved across the different subunits; however, structural variations in this binding site between subunits cannot be completely excluded.

Table 3: Gγ subunits structures created with VMD and AlphaFold server (www8). The residues 29 to 41 are marked in red.

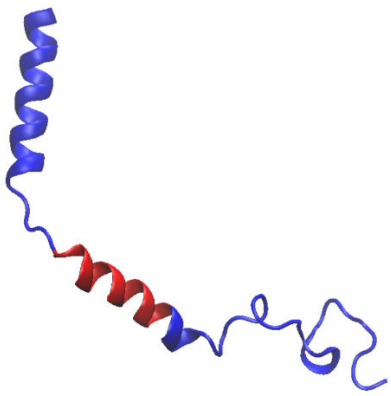 Gγ2 (4KFM | VMD)	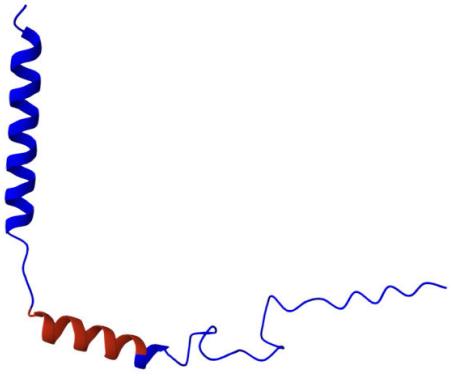 Gγ2 (AlphaFold)
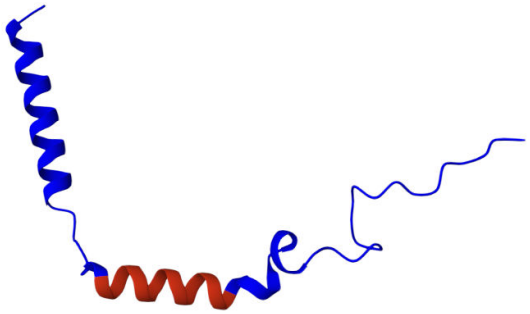 Gγ7 (AlphaFold)	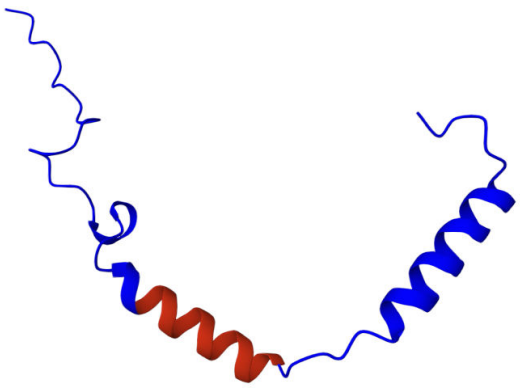 GγT2/Gγ9 (AlphaFold)

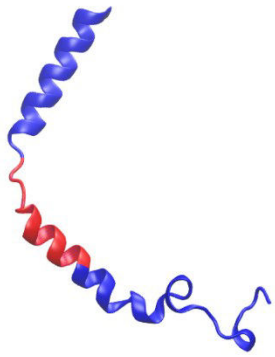 GγT1/Gγ1 (5KDO | VMD)	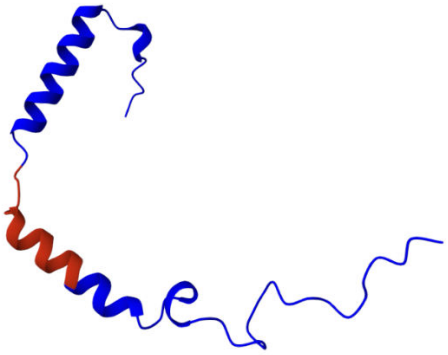 GγT1/Gγ1 (AlphaFold)
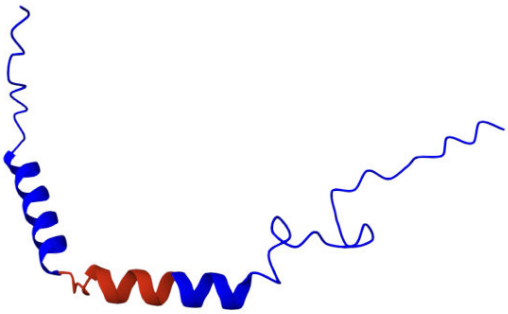 Gγ3 (AlphaFold)	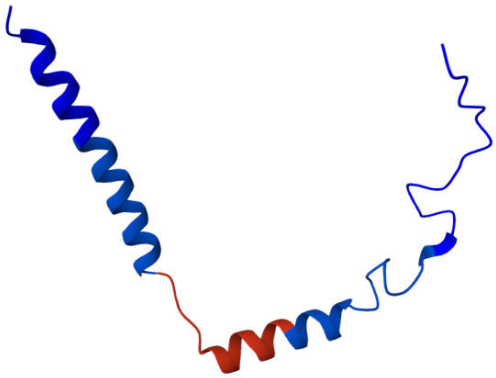 Gγ4 (AlphaFold)
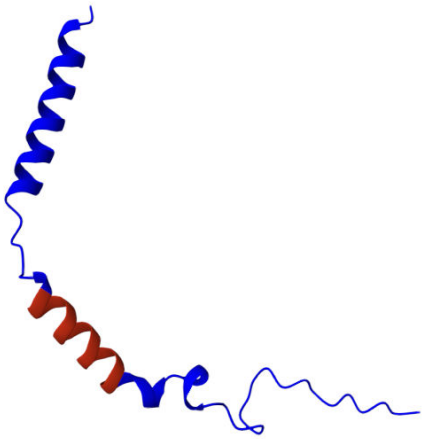 Gγ5 (AlphaFold)	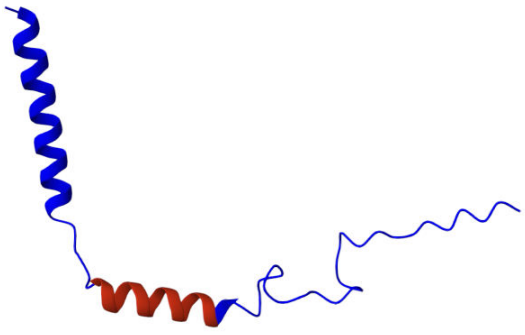 Gγ8 (AlphaFold)

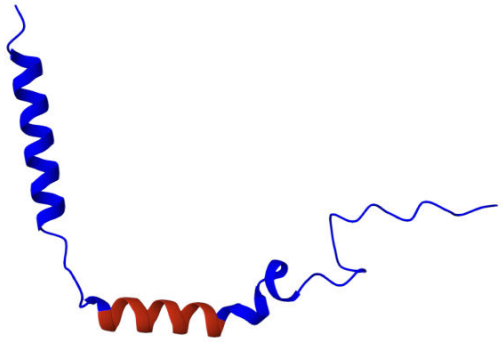

Gγ10 (AlphaFold)

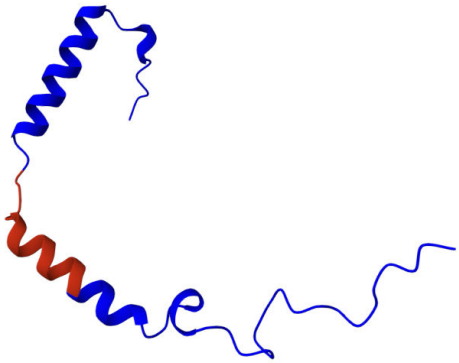

Gγ11 (AlphaFold)

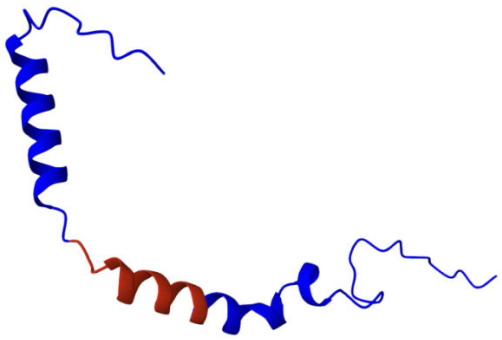

Gγ12 (AlphaFold)

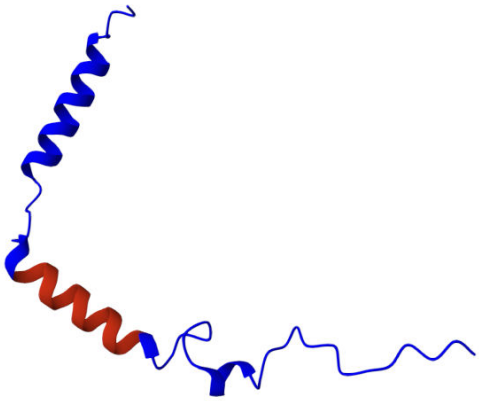

Gγ13 (AlphaFold)

The present data provide an initial overview of sequence variability among Gγ isoforms and highlight the importance of considering that a single mutation in Gβ1 may differentially affect its interaction with different Gγ subunits.

4 Results

The L30F mutation in the Gβ1 subunit of the G protein complex is associated with GNB1 encephalopathy. Molecular dynamics (MD) simulations were conducted to investigate its impact. The structure of the Gβγ subunit was retrieved from the Protein Data Bank (PDB ID: 4KFM). The objective was to understand the structural and dynamic effects of the L30F mutation on the stability of the Gβγ complex. We can draw conclusions about the impact of the mutation based on these results. The results are summarized below and discussed in more detail in the discussion section.

Based on the MD simulation data, free energy changes upon amino acid mutation (ΔΔG) were calculated. RMSD and RMSF were also analyzed following an extended MD run. Table 4 summarizes the simulation runs for the tripeptide, and Table 5 presents the same for the Gβγ subunit, all with the L30F mutation.

Table 4: MD Simulation Results for the Tripeptide

Run	**ΔG (kJ/mol)**
1	101,59 ± 0,35
2	101,76 ± 0,33
3	99,87 ± 0,33
4	101,10 ± 0,36
5	101,48 ± 0,33

The average ΔG value was calculated from the ΔG values from the five MD runs for the tripeptide.

$$\Delta G_{tripep}^{avg} = \frac{101{,}59 + 101{,}76 + 99{,}87 + 101{,}10 + 101{,}48}{5} = 101{,}16 \frac{kJ}{mol}$$

Table 5: MD Simulation Results for the Gβγ subunit

Run	ΔG (kJ/mol)
1	101,22 ± 0,96
2	101,83 ± 0,56
3	97,75 ± 0,71
4	96,40 ± 0,50
5	94,88 ± 0,74

4.1 Free Energy Calculation for the Tripeptide with the L30F Mutation

Figure 14 shows histograms generated from non-equilibrium molecular dynamics (NEMD) simulations of the tripeptide with the L30F mutation, along with ΔG values calculated using the Bennet acceptance ratio (BAR) method. These diagrams are representative snapshots. The free energy transformation from the wildtype to the L30F mutation and vice versa was calculated for the tripeptide model for five MD runs. The left side shows the work values for the forward and reverse transitions from the respective starting structures. On the right, histograms display the distributions of these work values. Here it is important that the two curves overlap. The intersection points of the distributions allow the calculation of the free energy difference.

Tripeptide Run 1	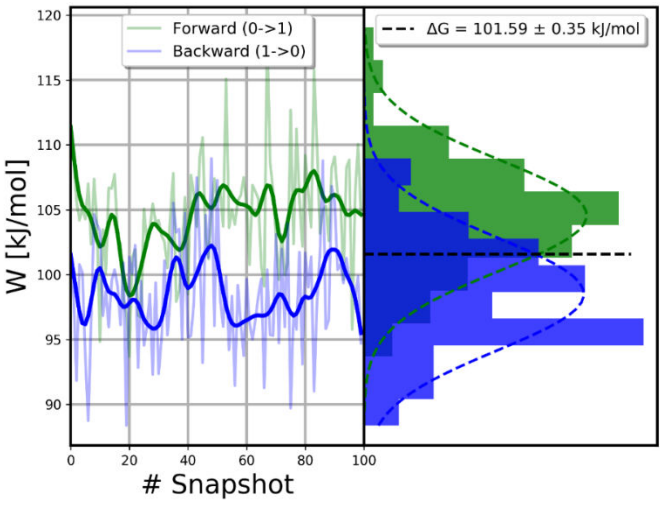

Tripeptide Run 2	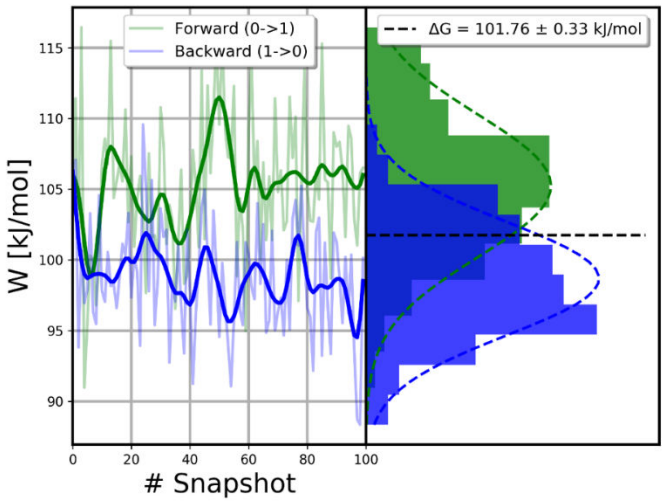
Tripeptide Run 3	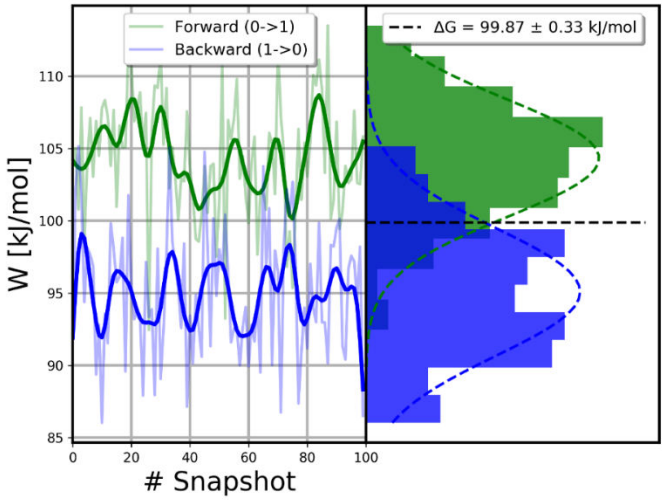
Tripeptide Run 4	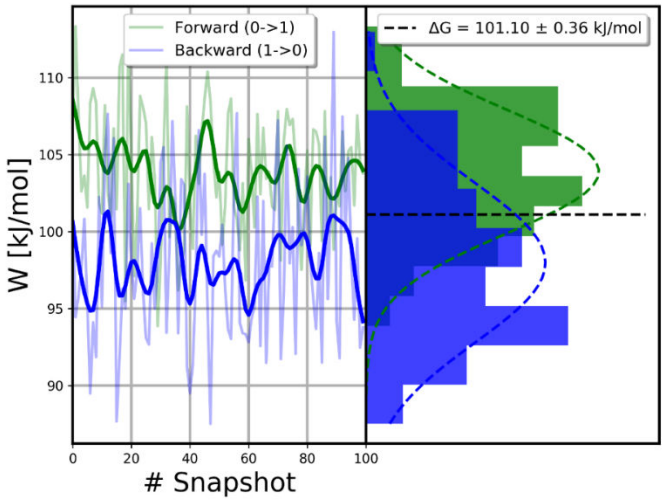

Tripeptide Run 5	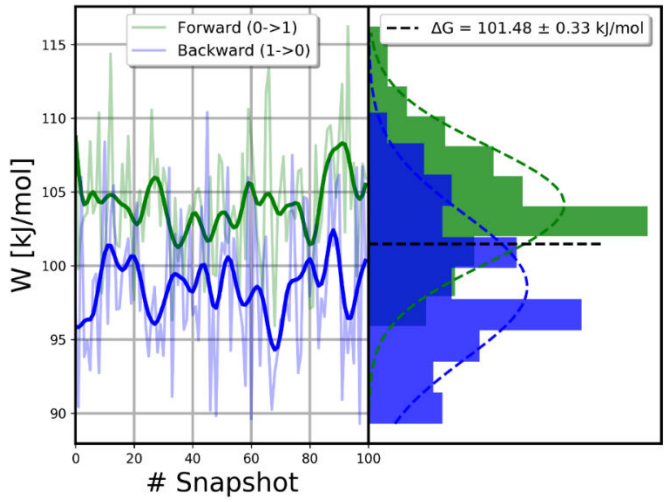

Figure 14: Free energy calculation for the tripeptide model with the L30F mutation. Left: Work values for forward (green) and reverse (blue) transitions (Y-axis = work; X-axis = number of snapshots). Right: Histogram of work value distributions.

4.2 Free Energy Calculation for the Gβ1γ2 Subunit with the L30F Mutation

Figure 15 presents the results for the Gβγ subunit using the same NEMD methodology and BAR calculations. The transformation free energies were calculated for five MD runs in both forward (WT → L30F) and reverse (L30F → WT) directions. As before, work value distributions and intersection points were used to determine the free energy difference.

Protein Run 1	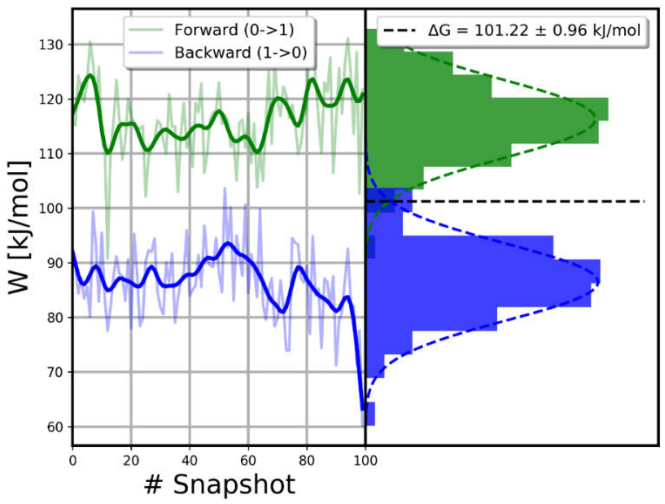

Protein Run 2	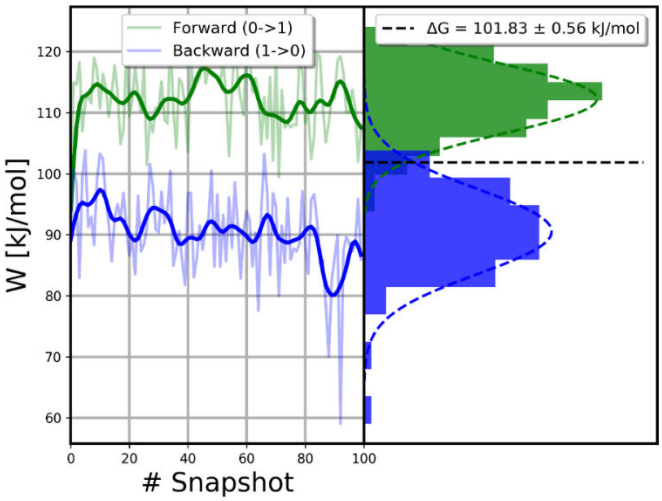
Protein Run 3	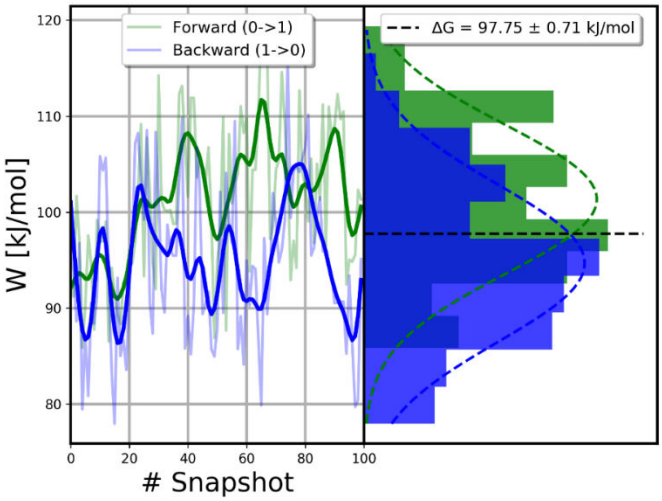
Protein Run 4	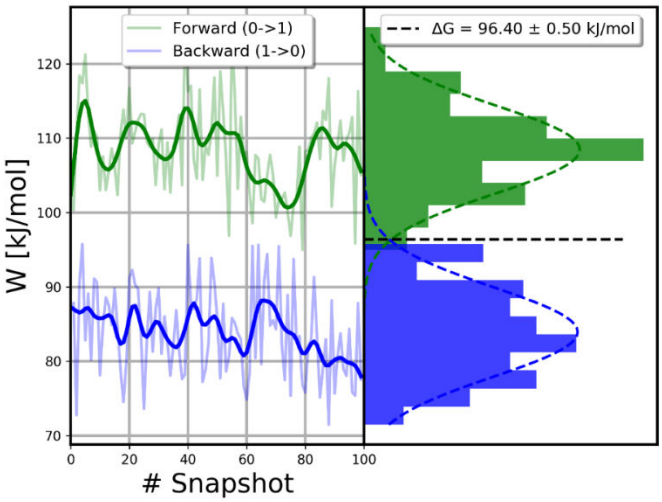

Protein Run 5	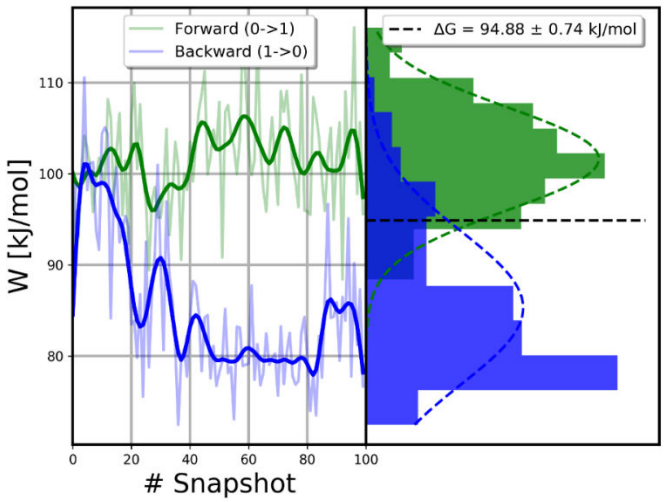

Figure 15: Free energy calculation for the Gβ1γ2 subunit with the L30F mutation. Left: Work values for forward (green) and reverse (blue) transitions (Y-axis = work; X-axis = number of snapshots). Right: Histogram of work value distributions.

4.3 ΔΔG Calculation Results

The ΔΔG values were calculated using the formula provided by Aldeghi et al. (2019), applied across all five MD runs. The results are summarized in Table 5.

$$\Delta\Delta G_{folding}^{mutation} = \Delta\Delta G^{protein} - \Delta G_{tripeptide}^{average} \quad (Aldeghi\ et\ al., 2019)$$

Table 6: Calculated ΔΔG Values

Run	ΔΔG (kJ/mol)
1	0,06
2	0,67
3	-3,41
4	-4,76
5	-6,28
Average ΔΔG: -2,74 kJ/mol	

The calculated average ΔΔG value for the L30F mutation is -2.74 kJ/mol. This average value suggests that the L30F mutation has a slight structural stabilizing effect on the Gβ1γ2 complex.

4.4 Root Mean Square Deviation (RMSD)

To further assess how the L30F mutation affects the Gß1y2 dimer, RMSD values were calculated for both the wildtype and mutant during a 250 ns extended MD run. Figure 16 illustrates these results.

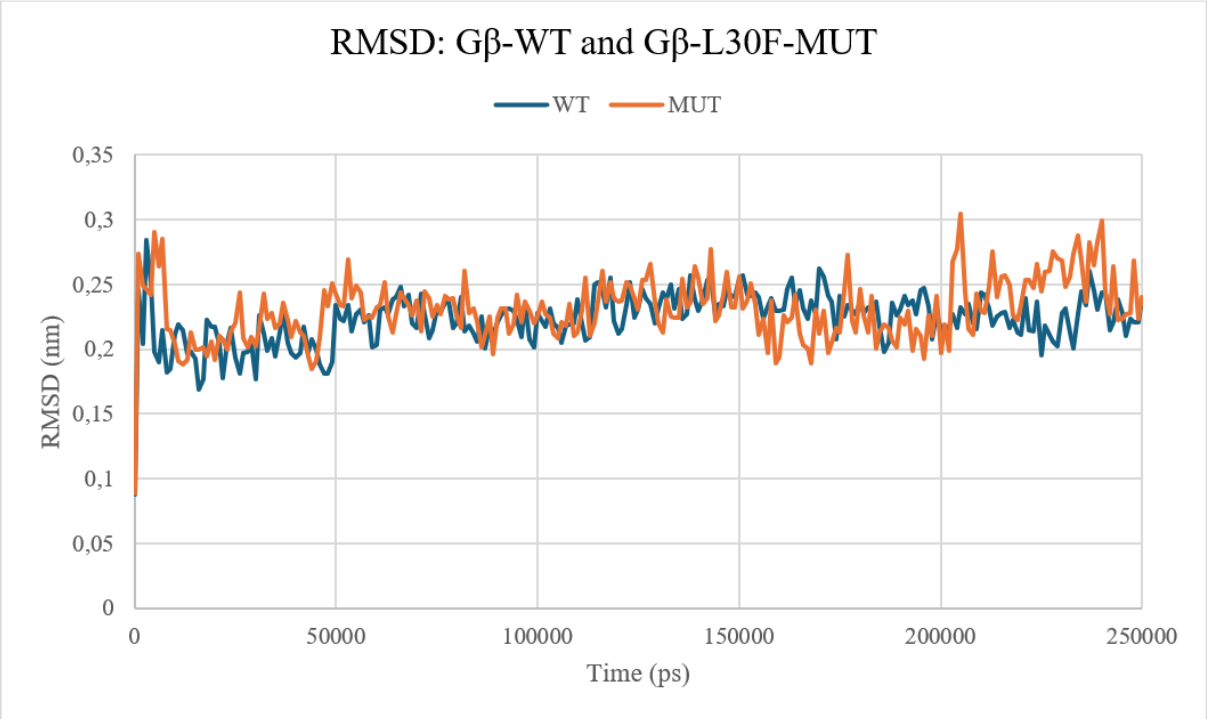

Figure 16: RMSD of the Gβ1 subunit for 250 ns MD simulation. Gβ1-L30F mutant in orange, Gβ1-wildtyp in blue.

Both the Gβ1-WT and Gβ1-L30F mutant show RMSD values predominantly between 0,19 nm and 0,26 nm, indicating structural stability. This data supports the hypothesis that this mutation does not significantly alter the dynamic properties of the protein.

4.5 Root Mean Square Fluctuation (RMSF)

RMSF values were also computed for both variants over the 250 ns simulation to assess local flexibility. RMSF identifies residues that remain flexible despite structural stabilization. Figure 17 shows RMSF results for the Gβ1-wildtype and the Gβ1-L30F-mutant.

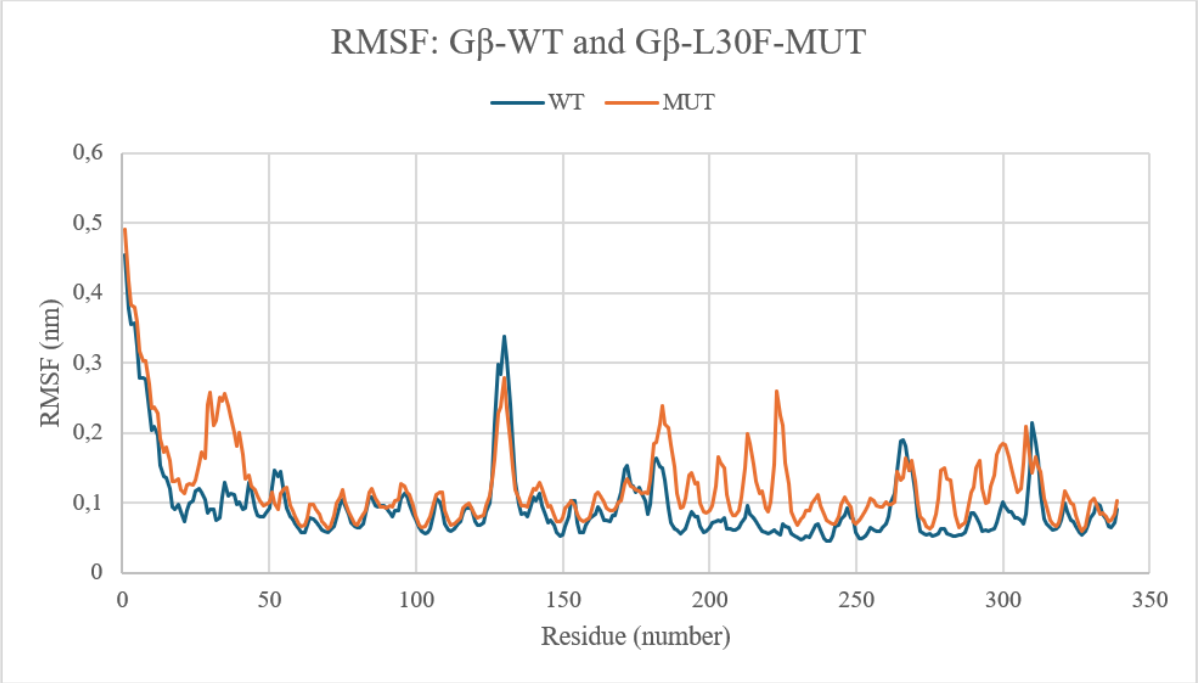

Figure 17: RMSF of the Gβ1 subunit for 250 ns MD simulation. Gβ1-L30F mutant in orange, Gβ1-wildtyp in blue.

The RMSF plot indicates that the Gβ1-WT and Gβ1-L30F mutant share a similar fluctuation profile, suggesting no major structural changes due to the mutation. However, some differences were observed in the flexibility of specific regions, particularly residues 30-35, 184-223, and 279-301.

4.6 Residue Energy Analysis

Energy interactions between L30F of Gβ1 and Gγ2 residues were calculated for both wildtype and mutant using the extended MD run 3. In Figure 18, the interactions during the final 50 ns of the simulation are shown, while Figure 19 presents the data for the entire 250 ns simulation period. Further, Figure 20 shows the Coulomb energy and Figure 21 shows the Lennard-Jones energy.

In the WT, four residues interact with L30F: Valine 30, Alanine 34, Leucine 37, and Methionine 38. Among these, Alanine 34 and Leucine 37 exhibit the strongest interaction energies. The negative interaction values indicate a stabilizing effect. In contrast, the mutant shows significantly weaker interactions, with only Alanine 34 showing a notable stabilizing effect. No other residues exhibit relevant interaction with the mutant.

These results suggest that the four residues, Val30, Ala34, Leu37, and Met38, play a crucial role in the stability of the protein and its interactions. Sequence alignment shows that these residues are the same in Gγ2 and Gγ7, making these two subunits well suited for comparison. In contrast, compatibility issues may arise when Gβ1 pairs with Gγ subunits that lack these conserved stabilizing residues.

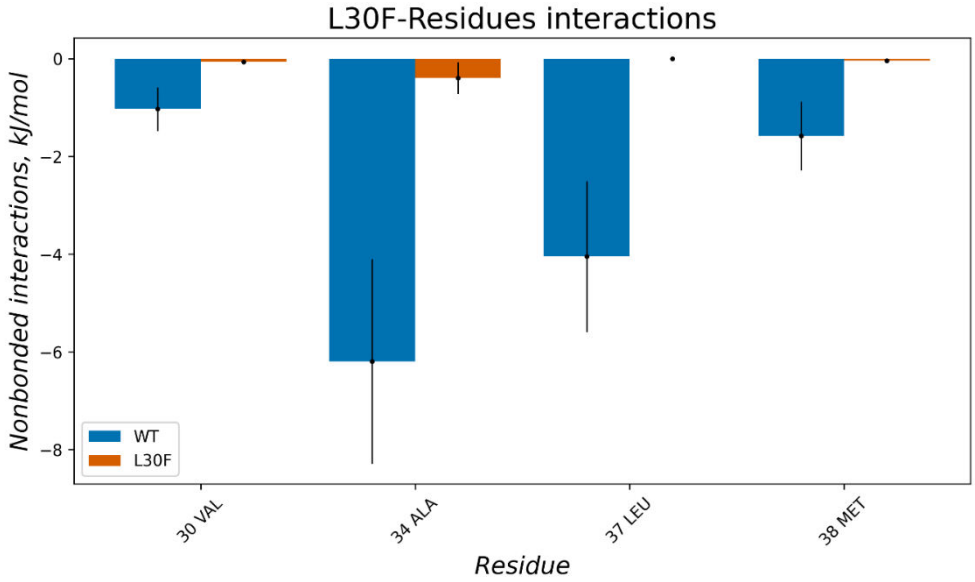

Figure 18: L30F-Residue interactions of the last 50 ns of the simulation process. Wildtype in blue, mutant in orange.

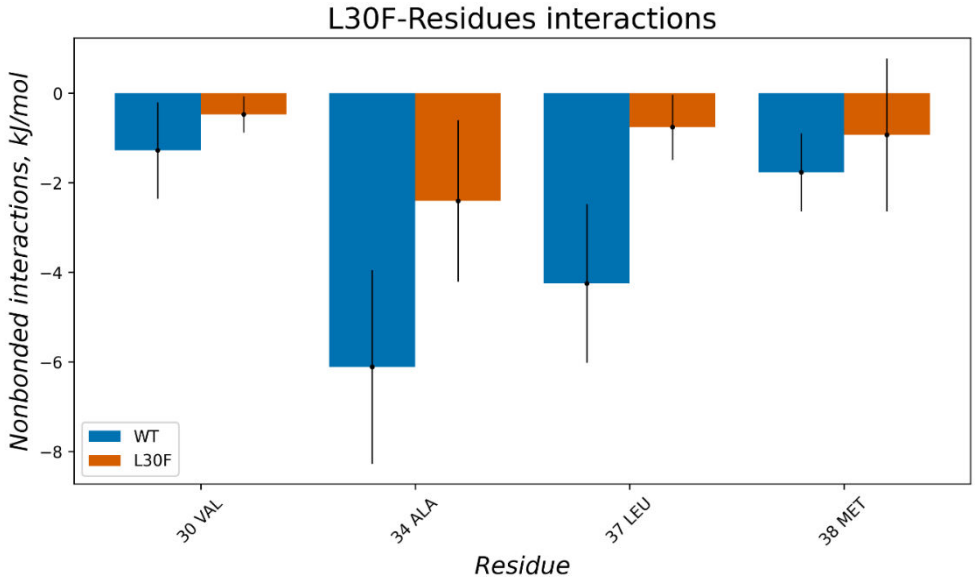

Figure 19: L30F-Residue interactions of the 250 ns simulation process. Wildtype in blue, mutant in orange.

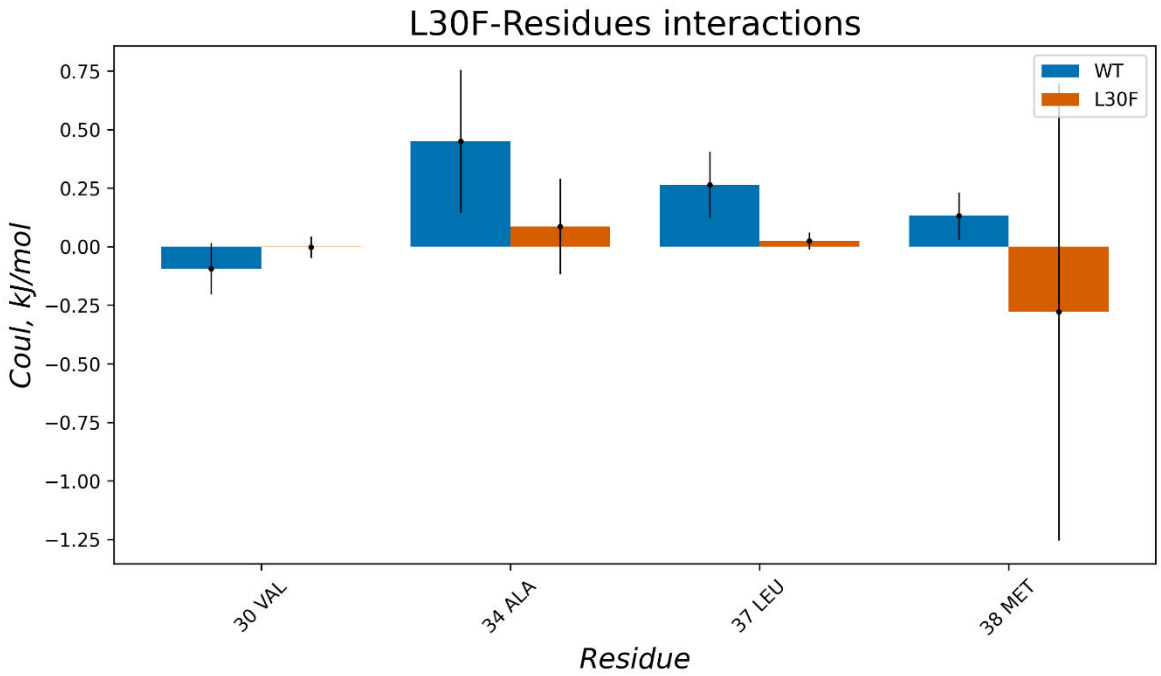

Figure 20: Coulomb energy for 250 ns simulation time for L30F-residues interactions.

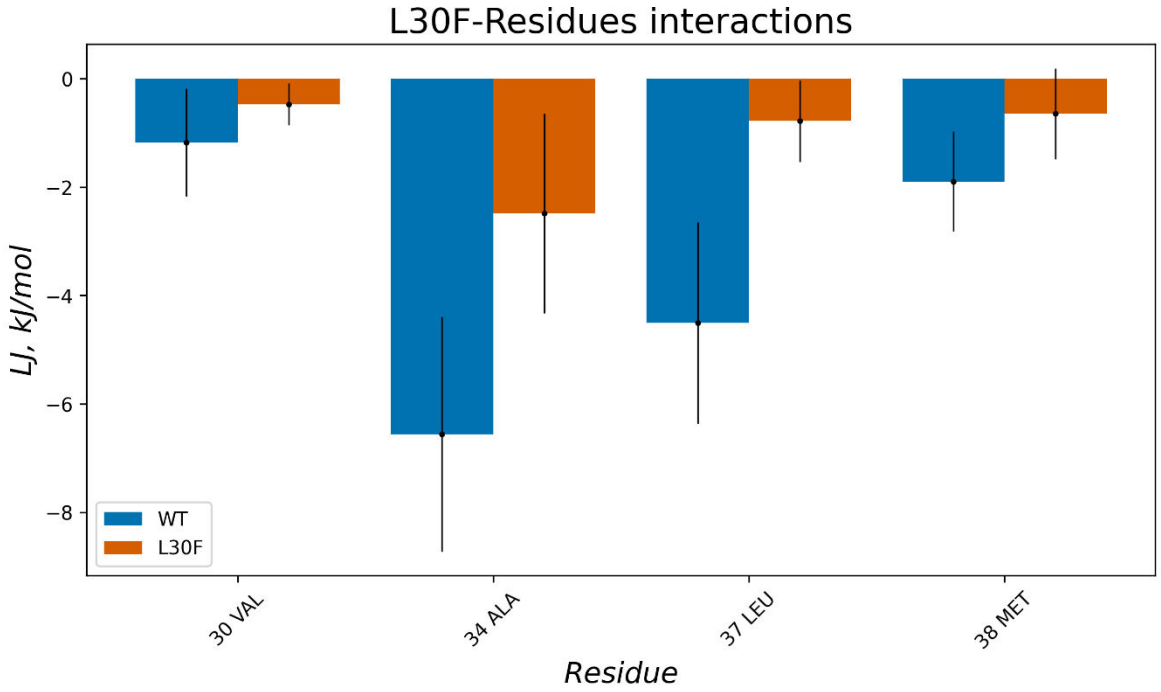

Figure 21: Lennard-Jones Energy for 250 ns simulation time for L30F-residues interactions.

We can now compare these four amino acids within the Gγ subunits (Figure 23). Residues 30, 34, and 37 are identical in most subunits, whereas residue 38 shows considerable variation among different subunits. It is possible that the occurrence of disease is related to specific interactions involving these residues in a particular subunit. It cannot be ruled out that, due to sequence differences in other Gγ subunits, additional amino acids may also be relevant for interactions between L30F in Gβ1 and Gγ. The largest change in amino acid sequence at critical residues (30, 34, 37, 38) corresponds to GγT2 (V30I, A34G, L37I, M38K), GγT1 (A34C, L37V, M38R), Gγ11 (A34S, L37I, M38K), Gγ13 (V30A, A34I), Gγ12 (A34S).

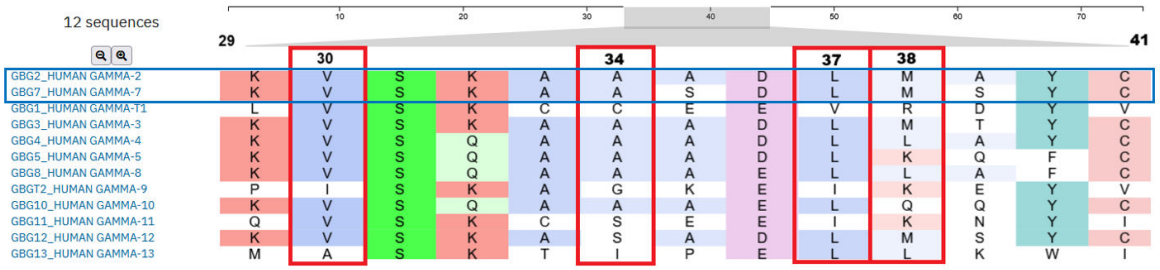

Figure 22: Comparison of residue 30, 34, 37 and 38 in Gγ subunits.

5 Discussion

GNB1 encephalopathy is a very rare neurodevelopmental disorder for which no targeted treatment is currently available. Existing therapeutic approaches are limited to symptomatic management. The clinical presentation associated with the L30F variant in the Gβ1 subunit seems to differ from other known pathogenic GNB1 mutations. Unlike all other reported cases, the patient carrying the L30F variant did not exhibit global developmental delay (GDD), which is typically observed in all other reported cases. Still, symptoms like muscular hypotonia, intellectual disability, seizures, nystagmus, and ataxia were present, aligning with the general phenotype of GNB1 encephalopathy.

To investigate the structural and dynamic effects of the L30F mutation, we carried out molecular dynamics (MD) simulations of the wildtype and mutant Gβγ complex. These included free energy change (ΔΔG) calculations, as well as RMSD and RMSF analyses, using the crystal structure 4KFM from the Protein Data Bank as a template.

We were able to analyze a few differences between wildtype and the L30F mutation. The average ΔΔG value of -2.74 kJ/mol suggests a slight stabilizing effect of the L30F mutation on the Gβ1γ2 complex. However, this value is very small, which suggests that it may not have any effect on stability. RMSD analyses showed overall structural stability; wildtype and L30F mutant are very similar, with only slight deviations observed in the final 50 ns of the 250 ns simulation. RMSF analysis indicated minor local fluctuations. Fluctuations were observed particularly at the residues 30-35 (near the mutation), as well as in the regions of residues 184-223 and 279-301. However, these probably have no influence on Gβγ stability.

It's worth mentioning that we only analyzed a single simulation run for RMSD and RMSF. Additional or longer runs would be needed to increase confidence in these results.

Our findings are consistent with those reported by Lohmann et al. (2017), who showed in functional assays that the L30F variant behaves similarly to the wildtype Gβ1. Their data indicated no major disruptions in dimer Gβ1γ7 or trimer $G\alpha_{olf}\beta1\gamma7$ formation. This supports the idea that the L30F mutation likely does not impair the overall stability of the Gβ1γ2 / Gβ1γ7 complex.

Looking more closely at residue-residue interactions, L30 was found to interact with Val30, Ala34, Leu37, and Met38 in Gγ2-residues that may contribute to complex stability. In the mutant, no strong interactions were observed between F30 and other residues in Gγ2. This might mean that the mutation does not have much impact on interactions with Gγ2, as well as Gγ7 because they have the same residues in these positions. But it is still possible that effects arise in the context of other Gγ subunits with different residues in this region.

Potential targets in case of L30F mutation are presumably GγT2, GγT1, Gγ11, Gγ13, Gγ12. Which may disrupt the correct Gβ1-Gγ interaction due to the change in amino acid sequence compared to Gγ2 and Gγ7.

6 Conclusion

This work represents a first step toward better understanding the structural and dynamic effects of the L30F mutation in the Gβ1γ2 complex. Molecular dynamics simulations suggest that the mutation does not significantly disrupt the stability of the Gβ1γ2 dimer. This is consistent with previous Gβ1γ7 studies (Lohmann et al., 2017).

To better understand GNB1 encephalopathy and its diverse clinical presentations, more comprehensive and prolonged MD simulations are necessary. It is important to distinguish between different types of GNB1 mutations, as their phenotypic outcomes may vary. Since no curative treatment exists, a more profound understanding of the underlying molecular mechanisms is essential for developing targeted therapeutic approaches.

Overall, our findings suggest that the L30F mutation does not impair Gβ1γ2 complex stability. The pathological effect of the L30F mutation is most likely associated with a disruption in the formation between the Gβ1 and GγT2, GγT1, Gγ11, Gγ13, Gγ12.

7 References

Adcock, S. A., & McCammon, J. A. (2006). Molecular dynamics: survey of methods for simulating the activity of proteins. *Chemical reviews*, *106*(5), 1589–1615. https://doi.org/10.1021/cr040426m

Aldeghi, M., de Groot, B. L., & Gapsys, V. (2019). Accurate Calculation of Free Energy Changes upon Amino Acid Mutation. In *Methods in Molecular Biology* (Vol. 1851, pp. 19–47). Humana Press Inc. https://doi.org/10.1007/978-1-4939-8736-8_2

Atkins, C. (2014). The physics of Poohsticks. *Physics World*, *27*(6), 56–56. https://doi.org/10.1088/2058-7058/27/06/46

Bai, X. chen, McMullan, G., & Scheres, S. H. W. (2015). How cryo-EM is revolutionizing structural biology. In *Trends in Biochemical Sciences* (Vol. 40, Issue 1, pp. 49–57). Elsevier Ltd. https://doi.org/10.1016/j.tibs.2014.10.005

Bassani, D., & Moro, S. (2023). Past, Present, and Future Perspectives on Computer-Aided Drug Design Methodologies. In *Molecules* (Vol. 28, Issue 9). Multidisciplinary Digital Publishing Institute (MDPI). https://doi.org/10.3390/molecules28093906

Betke, K. M., Rose, K. L., Friedman, D. B., Baucum, A. J., Hyde, K., Schey, K. L., & Hamm, H. E. (2014). Differential localization of G protein βγ subunits. *Biochemistry*, *53*(14), 2329–2343. https://doi.org/10.1021/bi500091p

Bledsoe, I. O., Viser, A. C., & Luciano, M. S. (2020). *Treatment of Dystonia: Medications, Neurotoxins, Neuromodulation, and Rehabilitation*. https://doi.org/10.1007/s13311-020-00944-0/Published

Colombo, S., Reddy, H. P., Petri, S., Williams, D. J., Shalomov, B., Dhindsa, R. S., Gelfman, S., Krizay, D., Bera, A. K., Yang, M., Peng, Y., Makinson, C. D., Boland, M. J., Frankel, W. N., Goldstein, D. B., & Dascal, N. (2023). Epilepsy in a mouse model of GNB1 encephalopathy arises from altered potassium (GIRK) channel signaling and is alleviated by a GIRK inhibitor. *Frontiers in Cellular Neuroscience*, *17*. https://doi.org/10.3389/fncel.2023.1175895

De Vivo, M., Masetti, M., Bottegoni, G., & Cavalli, A. (2016). Role of Molecular Dynamics and Related Methods in Drug Discovery. In *Journal of Medicinal Chemistry* (Vol. 59, Issue 9, pp. 4035–4061). American Chemical Society. https://doi.org/10.1021/acs.jmedchem.5b01684

Gapsys, V., Michielssens, S., Seeliger, D., & de Groot, B. L. (2015). pmx: Automated protein structure and topology generation for alchemical perturbations. *Journal of Computational Chemistry*, *36*(5), 348–354. https://doi.org/10.1002/jcc.23804

Guo, Y., Waldron, G. J., & Murrell-Lagnado, R. (2002). A role for the middle C terminus of G-protein-activated inward rectifier potassium channels in regulating gating. *Journal of Biological Chemistry*, *277*(50), 48289–48294. https://doi.org/10.1074/jbc.M207987200

Hamm, H. E. (1998). The many faces of G protein signaling. In *Journal of Biological Chemistry* (Vol. 273, Issue 2, pp. 669–672). https://doi.org/10.1074/jbc.273.2.669

Hemati, P., Revah-Politi, A., Bassan, H., Petrovski, S., Bilancia, C. G., Ramsey, K., Griffin, N. G., Bier, L., Cho, M. T., Rosello, M., Lynch, S. A., Colombo, S., Weber, A., Haug, M., Heinzen, E. L., Sands, T. T., Narayanan, V., Primiano, M., Aggarwal, V. S., … Anyane-Yeboa, K. (2018). Refining the phenotype associated with GNB1 mutations: Clinical data on 18 newly identified patients and review of the literature. *American Journal of Medical Genetics, Part A*, *176*(11), 2259–2275. https://doi.org/10.1002/ajmg.a.40472

Hollingsworth, S. A., & Dror, R. O. (2018). Molecular Dynamics Simulation for All. In *Neuron* (Vol. 99, Issue 6, pp. 1129–1143). Cell Press. https://doi.org/10.1016/j.neuron.2018.08.011

Jarzynski, C. (1997). *Nonequilibrium Equality for Free Energy Differences*. https://doi.org/10.1103/PhysRevLett.78.2690

Jo, S., Kim, T., Iyer, V. G., & Im, W. (2008). CHARMM-GUI: A web-based graphical user interface for CHARMM. *Journal of Computational Chemistry*, *29*(11), 1859–1865. https://doi.org/10.1002/jcc.20945

Kankanamge, D., Tennakoon, M., Karunarathne, A., & Gautam, N. (2022). G protein gamma subunit, a hidden master regulator of GPCR signaling. In *Journal of Biological Chemistry* (Vol. 298, Issue 12). American Society for Biochemistry and Molecular Biology Inc. https://doi.org/10.1016/j.jbc.2022.102618

Karplus, M., & McCammon, J. A. (2002). Molecular dynamics simulations of biomolecules. *Nature structural biology*, *9*(9), 646–652. https://doi.org/10.1038/nsb0902-646

Kolesnikov, A. v., Lobysheva, E., Gnana-Prakasam, J. P., Kefalov, V. J., & Kisselev, O. G. (2022). Regulation of rod photoreceptor function by farnesylated G-protein γ-subunits. *PLoS ONE*, *17*(8 August). https://doi.org/10.1371/journal.pone.0272506

Lazim, R., Suh, D., & Choi, S. (2020). Advances in molecular dynamics simulations and enhanced sampling methods for the study of protein systems. In *International Journal of Molecular Sciences* (Vol. 21, Issue 17, pp. 1–20). MDPI AG. https://doi.org/10.3390/ijms21176339

Lohmann, K., Masuho, I., Patil, D. N., Baumann, H., Hebert, E., Steinrücke, S., Trujillano, D., Skamangas, N. K., Dobricic, V., Hüning, I., Gillessen-Kaesbach, G., Westenberger, A., Savic-Pavicevic, D., Münchau, A., Oprea, G., Klein, C., Rolfs, A., & Martemyanov, K. A. (2017). Novel GNB1 mutations disrupt assembly and function of G protein heterotrimers and cause global developmental delay in humans. *Human Molecular Genetics*, *26*(6), 1078–1086. https://doi.org/10.1093/hmg/ddx018

Müller-Esterl, Werner: *Biochemie. Eine Einführung für Mediziner und Naturwissenschaftler*. 3. Auflage. Berlin, Heidelberg: Springer Spektrum (2018). XX + 740 S. (inkl. 1059 Abb.). – Online-Ressource. – DOI: 10.1007/978-3-662-54851-6. https://doi.org/10.1007/978-3-662-54851-6

Nasvytis, M., Čiauškaitė, J., & Jurkevičienė, G. (2024). GNB1 Encephalopathy: Clinical Case Report and Literature Review. *Medicina (Lithuania)*, *60*(4). https://doi.org/10.3390/medicina60040589

Ong, O. C., Hu, K., Rong, H., Lee, R. H., & K-K Fung, B. (1997). Gene Structure and Chromosome Localization of the G&ggr;c Subunit of Human Cone G-Protein (GNGT2). In GENOMICS (Vol. 44).

Petrovski, S., Küry, S., Myers, C. T., Anyane-Yeboa, K., Cogné, B., Bialer, M., Xia, F., Hemati, P., Riviello, J., Mehaffey, M., Besnard, T., Becraft, E., Wadley, A., Politi, A. R., Colombo, S., Zhu, X., Ren, Z., Andrews, I., Dudding-Byth, T., … Goldstein, D. B. (2016). Germline de Novo Mutations in GNB1 Cause Severe Neurodevelopmental Disability, Hypotonia, and Seizures. *American Journal of Human Genetics*, *98*(5), 1001–1010. https://doi.org/10.1016/j.ajhg.2016.03.011

Reddy, H. P., Yakubovich, D., Keren-Raifman, T., Tabak, G., Tsemakhovich, V. A., Pedersen, M. H., Shalomov, B., Colombo, S., Goldstein, D. B., Javitch, J. A., Bera, A. K., & Dascal, N. (2021). Encephalopathy-causing mutations in Gβ1 (GNB1) alter regulation of neuronal GIRK channels. *IScience*, *24*(9). https://doi.org/10.1016/j.isci.2021.103018

Revah-Politi, A., Sands, T.T., Colombo, S., Goldstein, D.B., and Anyane-Yeboa, K. (2020). GNB1 Encephalopathy. In: Adam, M.P., Feldman, J., Mirzaa, G.M., et al. (eds) Gene Reviews [Internet]. University of Washington, Seattle, 1993–2021. https://www.ncbi.nlm.nih.gov/books/NBK554743/

Smrcka, A. v. (2008). G protein βγ subunits: Central mediators of G protein-coupled receptor signaling. In *Cellular and Molecular Life Sciences* (Vol. 65, Issue 14, pp. 2191–2214). https://doi.org/10.1007/s00018-008-8006-5

Seeliger, D., & de Groot, B. L. (2010). Protein thermostability calculations using alchemical free energy simulations. *Biophysical Journal*, *98*(10), 2309–2316. https://doi.org/10.1016/j.bpj.2010.01.051

Serra, E., Ghidini, A., Decherchi, S., & Cavalli, A. (2025). Nonequilibrium Binding Free Energy Simulations: Minimizing Dissipation. *Journal of Chemical Theory and Computation*. https://doi.org/10.1021/acs.jctc.4c01453

Sondek, J., Bohm, A., Lambright, D. G., Hamm, H. E., & Sigler, P. B. (1996). *Crystal structure of a GA protein 0 py dimer at 2.1A resolution*. https://doi.org/10.1038/379369a0

Spring DJ, Neer EJ. (1994). A 14-amino acid region of the G protein gamma subunit is sufficient to confer selectivity of gamma binding to the beta subunit. J Biol Chem. 1994 Sep 9;269(36):22882-6. PMID: 8077239.

Tennakoon, M., Senarath, K., Kankanamge, D., Ratnayake, K., Wijayaratna, D., Olupothage, K., Ubeysinghe, S., Martins-Cannavino, K., Hébert, T. E., & Karunarathne, A. (2021). Subtype-dependent regulation of Gβγ signalling. In *Cellular Signalling* (Vol. 82). Elsevier Inc. https://doi.org/10.1016/j.cellsig.2021.109947

Thaker, T. M., Kaya, A. I., Preininger, A. M., Hamm, H. E., & Iverson, T. M. (2012). Allosteric mechanisms of G protein-coupled receptor signaling: A structural perspective. *Methods in Molecular Biology*, *796*, 133–174. https://doi.org/10.1007/978-1-61779-334-9_8

Whorton, M. R., & MacKinnon, R. (2013). X-ray structure of the mammalian GIRK2-βγ G-protein complex. *Nature*, *498*(7453), 190–197. https://doi.org/10.1038/nature12241

Wootten, D., Christopoulos, A., Marti-Solano, M., Babu, M. M., & Sexton, P. M. (2018). Mechanisms of signalling and biased agonism in G protein-coupled receptors. In *Nature Reviews Molecular Cell Biology* (Vol. 19, Issue 10, pp. 638–653). Nature Publishing Group. https://doi.org/10.1038/s41580-018-0049-3

Xiong, H., Crespo, A., Marti, M., Estrin, D., & Roitberg, A. E. (2006). Free energy calculations with non-equilibrium methods: Applications of the Jarzynski relationship. *Theoretical Chemistry Accounts*, *116*(1–3), 338–346. https://doi.org/10.1007/s00214-005-0072-2

8 Internet References

www1: GNB1 Foundation, Retrieved June 24, 2025; https://www.gnb1.org/

www2: MolView., Retrieved June 19, 2025; https://app.molview.com/

www3: Practical considerations for Molecular Dynamics, Retrieved July 22, 2025; https://computecanada.github.io/molmodsim-md-theory-lesson-novice/01-Force_Fields_and_Interactions/index.html

www4: pmx, Retrieved January 15, 2025; http://pmx.mpibpc.mpg.de/

www5: PDB, Protein Data Bank, Retrieved June 30, 2025; https://www.rcsb.org/structure/4KFM

www6: UniProt database, Retrieved July 30, 2025; https://www.uniprot.org/

www7: EMBL-EBI. *MAFFT multiple sequence alignment tool*. European Bioinformatics Institute, Retrieved August 5, 2025; https://www.ebi.ac.uk/Tools/msa/mafft/

www8: AlphaFold server, Retrieved August 5, 2025; https://alphafoldserver.com/

9 Supplementary Material

Gγ subunits amino acid sequences from UniProt database (https://www.uniprot.org/), FASTA format:

>sp|P63211|GBG1_HUMAN Guanine nucleotide-binding protein G(T) subunit gamma-T1 OS=Homo sapiens OX=9606 GN=GNGT1 PE=1 SV=2
MPVINIEDLTEKDKLKMEVDQLKKEVTLERMLVSKCCEEVRDYVEERSGEDPLV KGIPEDKNPFKELKGGCVIS
>sp|P59768|GBG2_HUMAN Guanine nucleotide-binding protein G(I)/G(S)/G(O) subunit gamma-2 OS=Homo sapiens OX=9606 GN=GNG2 PE=1 SV=2
MASNNTASIAQARKLVEQLKMEANIDRIKVSKAAADLMAYCEAHAKEDPLLTP VPASENPFREKKFFCAIL
>sp|P63215|GBG3_HUMAN Guanine nucleotide-binding protein G(I)/G(S)/G(O) subunit gamma-3 OS=Homo sapiens OX=9606 GN=GNG3 PE=1 SV=1
MKGETPVNSTMSIGQARKMVEQLKIEASLCRIKVSKAAADLMTYCDAHACEDP LITPVPTSENPFREKKFFCALL
>sp|P50150|GBG4_HUMAN Guanine nucleotide-binding protein G(I)/G(S)/G(O) subunit gamma-4 OS=Homo sapiens OX=9606 GN=GNG4 PE=1 SV=1
MKEGMSNNSTTSISQARKAVEQLKMEACMDRVKVSQAAADLLAYCEAHVRED PLIIPVPASENPFREKKFFCTIL
>sp|P63218|GBG5_HUMAN Guanine nucleotide-binding protein G(I)/G(S)/G(O) subunit gamma-5 OS=Homo sapiens OX=9606 GN=GNG5 PE=1 SV=3
MSGSSSVAAMKKVVQQLRLEAGLNRVKVSQAAADLKQFCLQNAQHDPLLTGV SSSTNPFRPQKVCSFL
>sp|O60262|GBG7_HUMAN Guanine nucleotide-binding protein G(I)/G(S)/G(O) subunit gamma-7 OS=Homo sapiens OX=9606 GN=GNG7 PE=1 SV=1
MSATNNIAQARKLVEQLRIEAGIERIKVSKAASDLMSYCEQHARNDPLLVGVPAS ENPFKDKKPCIIL

>sp|Q9UK08|GBG8_HUMAN Guanine nucleotide-binding protein G(I)/G(S)/G(O) subunit gamma-8 OS=Homo sapiens OX=9606 GN=GNG8 PE=1 SV=1
MSNNMAKIAEARKTVEQLKLEVNIDRMKVSQAAAELLAFCETHAKDDPLVTPV PAAENPFRDKRLFCVLL
>sp|O14610|GBGT2_HUMAN Guanine nucleotide-binding protein G(I)/G(S)/G(O) subunit gamma-T2 OS=Homo sapiens OX=9606 GN=GNGT2 PE=1 SV=1
MAQDLSEKDLLKMEVEQLKKEVKNTRIPISKAGKEIKEYVEAQAGNDPFLKGIP EDKNPFKEKGGCLIS
>sp|P50151|GBG10_HUMAN Guanine nucleotide-binding protein G(I)/G(S)/G(O) subunit gamma-10 OS=Homo sapiens OX=9606 GN=GNG10 PE=1 SV=1
MSSGASASALQRLVEQLKLEAGVERIKVSQAAAELQQYCMQNACKDALLVGVP AGSNPFREPRSCALL
>sp|P61952|GBG11_HUMAN Guanine nucleotide-binding protein G(I)/G(S)/G(O) subunit gamma-11 OS=Homo sapiens OX=9606 GN=GNG11 PE=1 SV=1
MPALHIEDLPEKEKLKMEVEQLRKEVKLQRQQVSKCSEEIKNYIEERSGEDPLVK GIPEDKNPFKEKGSCVIS
>sp|Q9UBI6|GBG12_HUMAN Guanine nucleotide-binding protein G(I)/G(S)/G(O) subunit gamma-12 OS=Homo sapiens OX=9606 GN=GNG12 PE=1 SV=3
MSSKTASTNNIAQARRTVQQLRLEASIERIKVSKASADLMSYCEEHARSDPLLIGI PTSENPFKDKKTCIIL
>sp|Q9P2W3|GBG13_HUMAN Guanine nucleotide-binding protein G(I)/G(S)/G(O) subunit gamma-13 OS=Homo sapiens OX=9606 GN=GNG13 PE=1 SV=1
MEEWDVPQMKKEVESLKYQLAFQREMASKTIPELLKWIEDGIPKDPFLNPDLM KNNPWVEKGKCTIL